FATIGUE ASSESSMENT OF HADFIELD STEEL FOR MACHINERY COMPONENTS

Lappeenranta–Lahti University of Technology LUT

Master’s Programme in Mechanical Engineering, Master's thesis

2025

Teemu Kauhala

Examiners: Assistant Professor (Tenure Track) Masoud Moshtaghi

D. Sc. (Tech.) Mahdieh Safyari

ABSTRACT

Lappeenranta–Lahti University of Technology LUT

LUT School of Energy Systems

Mechanical Engineering

Teemu Kauhala

Fatigue assessment of Hadfield steel for machinery components

Master's thesis

2025

97 pages, 19 figures and 6 tables

Examiners: Assistant Professor (Tenure Track) Masoud Moshtaghi and D. Sc. (Tech.) Mahdieh Safyari

Keywords: fatigue, Hadfield steel, microstructure, SEM, EDS, microhardness, carbon content, high-cycle fatigue, low-cycle fatigue

The aim of this thesis was to evaluate the fatigue performance of Hadfield steels with differing stress amplitudes, and to examine the influence of microstructure on fatigue strength. An MTS servohydraulic testing machine was used to test two variants, one with a higher carbon (C) content and the other with a lower one under cyclic loading. Furthermore, energy-dispersive X-ray spectroscopy (EDS), optical microscopy, scanning electron microscopy (SEM), and hardness tests were employed as supporting materials for microstructural analysis.

The high-carbon (HC) specimen exhibited higher fatigue strength in both low and high-cycle regimes. In the low-cycle regime, the fatigue strength was found to be approximately 680-690 MPa, in comparison to 570-590 MPa for the low-carbon (LC) specimen. At high-cycle regime, the difference narrowed to approximately 25 MPa. The microstructural investigations confirmed that a combination of improved tensile properties in the HC specimen is the likely reason. Moreover, SEM and EDS analyses revealed the presence of segregated carbon along the grain boundaries of the HC specimen, the amount was not sufficient to reduce the fatigue performance below that of the LC specimen.

The results demonstrate that C plays a critical role in the fatigue performance of Hadfield steel. In the case of machinery components that are subject to higher stresses, higher amount of C is beneficial. In the high-cycle regime, a component with a lower quantity of C may perform better.

TIIVISTELMÄ

Lappeenrannan–Lahden teknillinen yliopisto LUT

LUTin energiajärjestelmien tiedekunta

Konetekniikka

Teemu Kauhala

Hadfield-teräksestä valmistettujen koneenosien väsymisanalyysi

Konetekniikan diplomityö

2025

97 sivua, 19 kuvaa ja 6 taulukkoa

Tarkastajat: Apulaisprofessori (Tenure Track -urapolku) Masoud Moshtaghi ja TkT Mahdieh Safyari

Avainsanat: väsyminen, Hadfield-teräs, mikrorakenne, SEM, EDS, mikrokovuus, hiilipitoisuus, korkean syklimäärän väsyminen, matalan syklimäärän väsyminen

Tässä opinnäytetyössä tarkasteltiin kahden eri Hadfield-teräksen väsymislujuutta eri jännitysamplitudeilla, ja arvioitiin väsymislujuuden riippuvuutta materiaalin mikrorakenteeseen. Näytekappaleista toisella oli korkeampi ja toisella matalampi hiilipitoisuus (C). MTS servohydraulista testilaitetta käytettiin väsytyskokeissa, ja mikrorakenteen analysointi toteutettiin kovuusmittauksilla sekä käyttämällä optista mikroskooppia, pyyhkäisyelektronimikroskooppia (SEM), ja energiadispersiivistä röntgenspektroskooppia (EDS).

Tulosten perusteella korkeahiilisen (HC) näytteen väsymislujuus oli suurempi matalilla-, ja korkeilla syklimäärillä. Matalilla syklimäärillä väsymislujuudeksi todettiin noin 680–690 MPa, vastaavasti matalahiilisen (LC) näytteen väsymislujuus oli noin 570–590 MPa. Suurilla syklimäärillä näytteiden välinen ero väsymislujuudessa kaventui noin 25 MPa:iin. Mikrorakenteen analysointi vahvisti, että HC näytteen korkeampi lujuus on todennäköisin syy. SEM- ja EDS-analyysit osoittivat hiilen segregaatiota raerajoilla, mutta hiilen määrä raerajoilla ei riittänyt heikentämään sen väsymiskestävyyttä LC näytteen tasolle.

Tulokset osoittivat, että C:llä on tärkeä rooli Hadfield-teräksen väsymiskestävyydessä. Koneenosissa, joihin vaikuttaa suuremmat jännitykset, hyötyvät suuremmasta C-pitoisuudesta. Korkeasyklisessä kuormituksessa puolestaan pienempi C-pitoisuus toimii todennäköisesti paremmin.

ACKNOWLEDGEMENTS

I express my deepest gratitude to LUT University for this opportunity, and for providing an environment that has made it possible for me to develop both personally and professionally. I am particularly grateful to my supervisor Masoud Moshtaghi and Mahdieh Safyari for providing guidance and feedback throughout this research.

I would also like to extend my profound appreciation to Antti Heikkinen whose invaluable help with test specimen preparation, hardness testing and the use of an optical microscope provided vital insight into the material under investigation. Additionally, I would like to thank Santeri Kurkinen and Donat Horvath for their help with SEM, without which it would have been exceedingly difficult to interpret the results of the fatigue tests.

Finally, I wish to thank my family for their support, and my employer for providing the flexibility and understanding that allowed me to balance the demands of writing my thesis with my professional responsibilities.

SYMBOLS AND ABBREVIATIONS

Roman characters

a	Initial crack size	mm
A	Area of the crack	mm^2
E	Young's modulus	MPa
E_{rel}	Relative Error	%
G	Energy release rate	J/m^2
H'	Cyclic hardening coefficient	MPa
K_I	Stress intensity factor for mode I	MPa√m
K_{II}	Stress intensity factor for mode II	MPa√m
K_{III}	Stress intensity factor for mode III	MPa√m
ΔK	Stress intensity factor range	MPa√m
ΔK_{eq}	Equivalent stress intensity factor range	MPa√m
l	Mean lineal intercept length	mm
L_T	True length of a test line	mm
M	Material parameter	-
N	Number of cycles	-
N_f	Number of cycles to failure	-
N^*_{mi}	Corrected fatigue life	-
$\bar{P}$	Mean value for number of intersections	-
R	Stress ratio	-
Y	Geometry dependent correction factor	-

Greek characters

γ	Walker parameter	-
γ_{max}	Maximum shear strain	-
$\Delta\varepsilon_p$	Plastic strain range	-
$\Delta\sigma$	Stress range	MPa
ε_{ar}	Completely reversed strain amplitude	-
ε'_f	Fatigue ductility coefficient	-
ε_p	Plastic strain component	-
μ	Shear modulus	MPa
Π	Potential energy	J
ρ	Notch root radius	mm
σ_a	Stress amplitude	MPa
σ_{ai}	Principal alternating nominal stress	MPa
σ_{ar}	Equivalent completely reversed stress amplitude	MPa
σ_{eq}	Equivalent stress	MPa
σ'_f	Fatigue strength coefficient	MPa
σ_m	Mean stress	MPa
σ_{max}	Maximum stress	MPa
σ_{min}	Minimum stress	MPa
σ_{net}	Stress at cross-section	MPa
$\sigma_{n,max}$	Maximum normal stress	MPa
σ_{nom}	Nominal stress	MPa
σ_{notch}	Fatigue limit stress in notched component	MPa
σ_{peak}	Peak stress at notch root	MPa

σ_{smooth}	Fatigue limit stress in smooth component	MPa
σ_{xy}	Crack front stress, mode II	MPa
σ_{y}	Yield strength	MPa
σ_{yy}	Crack front stress, mode I	MPa
σ_{yz}	Crack front stress, mode III	MPa

Constants

a^*	Material dependent constant	mm
C	Paris' law coefficient	-
κ_{FS}	Material constant	-

Dimensionless quantities

b	Fatigue strength exponent
Bi	Bismuth content
c	Fatigue ductility exponent
Cr	Chromium content
Cu	Copper content
Fe	Iron content
G	Grain size index
K_f	Fatigue notch factor
K_t	Stress concentration factor
m	Paris' law exponent
Mo	Molybdenum content
n	Number of applied load cycles

n'	Cyclic hardening exponent
N	Number of total cycles
Ni	Nickel content
P	Phosphorus content
q	Notch sensitivity
S	Sulphur content
Si	Silicon content
Ti	Titanium content
ν	Poisson's ratio
V	Vanadium content

Abbreviations

BSE	Backscattered Electron
CI	Confidence Interval
DSA	Dynamic Strain Aging
EDS	Energy-Dispersive X-ray Spectroscopy
EPMA	Electron Probe Microanalysis
ε-N Curve	Strain-Life curve
HC	High-Carbon
LC	Low-Carbon
LEFM	Linear Elastic Fracture Mechanics
SE	Secondary Electron
SEM	Scanning Electron Microscope
SFE	Stacking Fault Energy

SIF	Stress Intensity Factor
S-N Curve	Stress-Life curve
STD	Standard Deviation
SWT	Smith-Watson-Topper
WDS	Wavelength-Dispersive X-ray Spectroscopy
XRD	X-ray Diffraction

Table of contents

Figures

Tables

DECLARATIONS

Turnitin

The originality of this thesis has been reviewed with the Turnitin similarity checking service.

AI usage

The author of the thesis, Teemu Kauhala, used the following AI-tools during the preparation of the thesis:

1. DeepL Write with corrections only

    a. Purpose of use: Grammar improvement

    b. Explanation of the use of the tool: Improve the structure of the language with regard to punctuation and subject-verb agreement.

Responsibility

The author, Teemu Kauhala, takes full responsibility for the content of this thesis and has reviewed and edited the content generated by the possible use of AI tools.

1 Introduction

The role of fatigue as a cause of failure in machine components is argued to cover up to 90 % of all mechanical failures, making it one of the most important aspects to be considered during their design phase (Arghavan et al. 2011). A significant amount of research has been devoted to understanding how different materials respond to cyclic loading conditions, and subsequently, how the deleterious effects of fatigue can be mitigated to reduce the likelihood of fatigue failure of machine components. One such material is Hadfield steel, which is known for its wear resistance and widespread use in the machinery components, especially in the field of mining.

The structure of this thesis is divided into the following chapters. Chapter one introduces the objective of the work, including its scope and limitations. Chapter two is dedicated to the review of relevant literature, discussing the fatigue performance of Hadfield steels. Chapter three presents the theoretical framework and methodology consisting of characterisation of Hadfield steels properties and different fatigue assessment methods of machinery components. Chapter four is dedicated to presenting and discussing the results of the experimental fatigue tests and metallography. Chapter five concludes the thesis with summarising the key findings.

1.1 Objectives of the Thesis

The main objective of this thesis is to assess the fatigue performance of Hadfield steel with varying carbon contents. The fatigue performance is assessed through experimental fatigue testing of two cast Hadfield steel variants, one with a higher quantity of carbon (HC) and one low-carbon (LC). Experimental fatigue assessment is combined with microstructural investigation and hardness testing measurements. The focus under the main objective is to investigate the influence of carbon content on the fatigue performance in low-cycle and high-cycle fatigue regimes.

Additionally, this thesis aims to bridge the gap in research with regard to fatigue performance of Hadfield steel. A significant amount of research has been conducted into the wear performance of Hadfield steels, as well as the influence of microstructure on the tensile

properties and deformation mechanism, but only a small amount of research can be found related to fatigue, especially high-cycle fatigue. Combining experimental fatigue analysis with metallography, this thesis attempts to advance the knowledge of the fatigue performance of Hadfield steel.

1.2 Scope of the Thesis

The scope of this thesis entails an assessment of the fatigue performance of Hadfield steel through experimental testing. Fatigue testing will be conducted on two different cast Hadfield steel variants using an MTS servohydraulic fatigue test system. These variants differ from each other by their carbon content. Testing will be performed with different levels of stress and strain to determine the fatigue life of the material. The Vickers-hardness of the test specimens will also be measured. Furthermore, the two specimens will be investigated under both an optical microscope and SEM as well as EDS. The experimental test results will be analysed and compared with the findings of other similar research papers related to fatigue performance of Hadfield steel as well as subjects related to the microstructure and deformation behaviour.

1.3 Limitations of the Thesis

This thesis is limited to the study of base material fatigue performance and does not consider fatigue of welded structures. Excluding the effect of welding on fatigue performance enables the thesis to focus on the fatigue performance and behaviour of the Hadfield steel itself. Further, given the extensive compendium of fatigue assessment methods related to fatigue of base material, this thesis shall focus only on some of the most commonly utilized analytical approaches.

2 Literature review

The objective of this literature review is to examine existing studies on the fatigue performance of austenitic manganese steel, or more specifically Hadfield steel to get a better grasp of the material and its behaviour when subjected to a cyclic load, and to establish a foundation for the fatigue performance of Hadfield steel. The examined research papers focus on both low-cycle fatigue performance, as well as high-cycle fatigue performance. A detailed account of the fundamental concepts and definitions of fatigue will be presented in a subsequent chapter as a part of the theoretical framework of this thesis.

2.1 Low-Cycle Fatigue

Low-cycle fatigue is characterised by a relatively large amount of plastic deformation per applied load cycle. It is generally associated with a high stress magnitude and a low number of cycles to failure. A machinery component subject to high stresses may fail due to fatigue even after a thousand loading cycles, with most of the time spent in the crack propagation phase. In the low-cycle regime, fracture of the component can occur while the fatigue cracks are still small in size. (Schijve 2009, pp. 161-162.)

A total of three studies into low-cycle fatigue were reviewed. The first of which is by Schilke et al. (2010) who investigated the fatigue and deformation behaviour of austenitic manganese steels in both as-cast and rolled conditions. The team conducted low-cycle fatigue tests at three different levels of constant total strain amplitude between 0.4 and 1.0 % using a constant stress amplitude and strain rate. As a result of the fatigue tests, the team was able to conclude that both specimen variants behaved in a similar manner. At a 0.4 % strain amplitude, hardening takes up only a part of the fatigue life, and the material shows slight softening. At 0.6 %, the softening of the material increases for the entire fatigue life. The cast specimens exhibited a wide range of fatigue life due to porosity. Even though the cast specimens were more porous, due to their ductility, some of the cast specimens lasted as long as some of the rolled specimens, which contained little to no porosity. This phenomenon was explained by the fact that the ductility of the cast material reduced its sensitivity to defects. Furthermore, the study was able to conclude that the deformation behaviour of the

specimens did not show necking during monotonic loading, a general area reduction was observed instead. More specifically, work hardening did occur around these locally reduced regions. However, the rolled specimens showed larger elongation in comparison to cast specimens regardless of the fact that both specimens had relatively similar yield and ultimate strength.

Kang et al. (2014) published a study investigating the cyclic deformation and fatigue behaviour of Hadfield steel using a strain-controlled method. The test utilised plates with dimensions of 25 mm thick by 45 mm high forged specimens. The tests were done using an MTS servohydraulic testing machine with different strain amplitudes ranging from $3x10^{-3}$ to $1x10^{-2}$. The fatigue life was determined when the tensile stress decreased back to a magnitude 25 % below the peak stress. The study found that the material appears to show cyclic hardening initially, and then subsequent softening until failure. Further, the fatigue life of Hadfield steel under low-cycle fatigue testing depends in large part on the internal stress of the specimen. The internal stress resulted in a higher total stress amplitude along with a larger strain amplitude, resulting in a faster crack growth. The study also notes that as the primary mechanism of fatigue fracture is by quasi-cleavage in both low- and high-cycle fatigue, the behaviour of Hadfield steel is similar to other steels in so far as the mechanisms through which fatigue occurs is by cyclic plastic deformation, but for low-cycle fatigue especially, the deformation microstructure is the controlling factor in fatigue failure.

Another factor that determines the strength of Hadfield steel and consequently its fatigue strength is whether the specimen has been deliberately pre-hardened. Further, the method by which pre-hardening has been achieved appears to influence the fatigue life of a component. Chen et al. (2017) compared the low-cycle fatigue behaviour of a pre-hardened Hadfield steel to water-quenched Hadfield steel under different strain amplitudes at a constant strain rate. The study found that at similar strain amplitudes, the fatigue life of pre-hardened Hadfield steel was clearly longer compared to the fatigue life of water-quenched specimens. However, at high total strain amplitude, the difference in fatigue life was reversed where the water-quenched specimens had the advantage. The switch in fatigue life between pre-hardened and water quenched Hadfield steel after the total strain amplitude reached a certain threshold was attributed to the changing microstructure. At higher strain amplitude, the amount of dislocation motion increased, which in turn resulted in dislocation pileups at twin

boundaries and to an increase in stress concentration, whereas with lower strain amplitudes the dislocations could relax, thus improving the deformation capacity of the material.

2.2 High-Cycle Fatigue

High-cycle fatigue, as opposed to low-cycle fatigue, is characterised by a large number of load cycles with a relatively low stress amplitude. The applied stress is commonly above the fatigue limit, but below the yield strength of the material, meaning that deformation is largely elastic. Stresses in the elastic range result in significantly smaller plastic deformation, which is why fatigue failure in the high-cycle regime occurs due to an accumulation of microscopic damage. Most of the fatigue life is therefore spent on fatigue crack initiation, because it takes a substantial number of cycles until a sufficient amount of damage has accumulated on the surface of the specimen for a crack to initiate. For this reason, high-cycle fatigue can be measured in millions of load cycles. (Milella 2024, pp. 45-46.)

A total of five studies into high-cycle fatigue were reviewed. The same study by Kang et al. (2014) also investigated high-cycle fatigue behaviour of Hadfield steel under three-point bending and rotating bending loads. The high-cycle fatigue test was conducted with a frequency of 80 Hz and a load ratio of 0.1 until the specimen broke, or the test reached 10 million cycles. The results of the test revealed that the fatigue strength of the material is between 0.4 to 0.5 times the ultimate strength, and just under the value for the yield strength corresponding to the applied load type. For rotating bending, the fatigue limit was approximately 50 % lower than three-point bending, or 660 MPa. The higher fatigue strength in three-point bending was attributed to three parts, namely the applied stress ratio and stress distribution as well as the capacity of Hadfield steel to work-harden.

The second study focused on investigating the effect of cooling rate after heat treatment on the mechanical properties of Hadfield steel, including fatigue life. Cast ASTM A-128 austenitic Mn Hadfield steel blocks were austenitized for two hours and subsequently quenched. One of the blocks was quenched in water, and the other in 3 % wt.-% NaCl salt bath. The specimens were tested under bending using a stress ratio of -1 and an applied stress between 500 – 650 MPa at ambient temperature. The results of the study revealed that the sample that was quenched in a salt bath possessed a higher fatigue life, regardless of the magnitude of applied stress. The reason for the improved fatigue life was attributed to the

increased deformability in the plastic region at the tip of the fatigue crack, which slows the rate at which fatigue cracks grow. (Anijdan & Sabzi 2018.)

The third study into high-cycle fatigue, specifically focusing on the micromechanical behaviour of fatigue cracks in Hadfield steel, was published by Feng et al. (2013). The study analysed a railway crossing which contained a fatigue crack along the working surface. The fatigue cracks were formed by rolling contact as a result of multiple trains passing over the crossing. While studies into austenitic steels have previously shown that grain orientation has an effect on the direction of fatigue crack growth, no such correlation was found by Feng et. al. However, the study was able to observe the interaction between slipping dislocation and deformation twinning, and their effectiveness in preventing dislocation motion during plastic deformation. The link between slipping dislocation and deformation twinning is closely tied to the ability of the material to cyclically harden under rolling contact fatigue. As for crack propagation in the material, the team observed that the boundaries generated through twinning act as obstacles that hinder the growth of fatigue cracks.

The fourth study investigated a steel crossing nose made of Hadfield steel. Dhar et al. (2019) studied crack formation and microstructure of a damaged steel crossing nose. The test specimen was a piece from the Danish rail track where it had been exposed to variety of different loading conditions. The measured average axle load from traffic was approximately 14 tons with an average speed of 135 km/h. The team observed that fatigue cracks nucleated for the most part from the surface into the material along grain boundaries or along discontinuities that resulted in localised defects. The results also appeared to coincide with the findings of Feng et al. (2013) by confirming that accumulating strain has a greater influence on the crack growth orientation instead of grain orientation. The study also showed that the ability of Hadfield steel to harden due to work has a beneficial effect in delaying the failure of the component under cyclic loading. The delayed failure was largely influenced by the microstructure of the base material. The microstructure had a delaying effect on fatigue via twinning because it accommodates plastic deformation, and at the same time relates to strain hardening, resulting in a slower crack growth. As a results of the twin boundaries forming in the material, the growth of fatigue cracks appeared to slow down. Instead of propagating through the twin boundaries, the fatigue cracks grew through regions where such boundaries did not form which is why the growth of these cracks appeared to be delayed.

The fifth study focuses on rolling contact fatigue behaviour of Hadfield steel. Harzalla et al. (2010) examined water quenched, coarse-grained, X120Mn12 cast steel bars with 10 mm diameter. The samples were subjected to an axial load of 700 N, which resulted in a Hertzian contact pressure of 2200 MPa. Two different rotational speeds were used: 9 Hz and 46 Hz, for up to 150 000 cycles. The findings of the research revealed that the surface hardness of the contact surface increased as a function of applied cycles. The microhardness of the samples was initially approximately 400 HV, but after 50 000 cycles, it had doubled. At 150 000 cycles, the hardness on the surface of the sample reached approximately 1000 HV. Based on the microscopic investigation, the surface was divided into two regions, where the first one is approximately 200 µm thick and contains several micro-cracks in the contact zone. The second region is below the first, and it is approximately 400 µm thick and shows a high number of deformation twins. The microscopic investigation also concluded that fatigue cracks initiate from the surface and propagate downwards towards the core of the specimen.

3 Theoretical Framework and Methods

This chapter presents the theoretical framework of the thesis, and it begins with a look into austenitic manganese steels, specifically Hadfield steel, its chemical composition and mechanical properties. The second subchapter is dedicated to the phenomenon of fatigue and different interrelated aspects that influence the fatigue performance of machine components. The third subchapter focuses on fatigue assessment methods. As the field of fatigue assessment methods is vast and there exists multiple different theories and approaches, a comprehensive but not all-encompassing review of the most commonly used methods shall be introduced, including methods based on stress-life, strain-life and fracture mechanics. In addition to different fatigue assessment approaches, the effect of notches, variable amplitude loading as well as multiaxial fatigue will be introduced. The theoretical framework for this thesis consists of fatigue assessment methods pertaining to fatigue of base material only. The final subchapter in methods is used for explaining the setup for experimental fatigue and hardness testing as well as metallographic examination of Hadfield steel specimens.

3.1 Hadfield Steel

Hadfield steel or also known as Mangalloy, is a subset of austenitic manganese steels that was originally discovered by Robert Hadfield in 1882. According to a copy of one of Hadfield's US patents, namely patent number 303,151 published in 1883, Hadfield steel is defined as steel with manganese (Mn) content between 7 to 30 %. (Kirk 2023.) More modernly, however, variations of Hadfield steel have been patented, resulting in multiple different versions and definitions of what the term Hadfield steel constitutes. For example, the range of Mn content has commonly been agreed to be between 11 – 14 % (US 8,753,565 B2, 2014).

3.1.1 Chemical Composition

Hadfield steel is still a very popular material today despite being discovered over 140 years ago. It is extensively used in industries related to mining, drilling, steelmaking, railroading

and many other industries due to its unique properties. The versatility of Hadfield steel comes from its ability to withstand wear exceptionally well. Moreover, the steel is capable of work-hardening to a great degree by hammering, explosion shocking or pressing resulting in a very hard wear resistant surface layer. (Subramanyam et al. 1990, p. 1951.)

The material composition of austenitic manganese steel changes based on the intended application. With small changes to the proportion of carbon (C) and Mn as well as by adding various alloys such as chromium (Cr), vanadium (V), molybdenum (Mo), titanium (Ti) and others can greatly improve the resulting product. Some commonly used grades are presented in Table 1.

Table 1. Typical composition of common austenitic manganese steels (Subramanyam et al. 1990, pp. 1951-1952, Adapted)

Grade (ASTM, A 128)	**C (%)**	**Mn (%)**	**Cr (%)**	**Mo (%)**	**Ni (%)**	**Si (%)**	**P (%)**
A	1.05-1.35	11.0	-	-	-	1.00	0.07
C	1.05-1.35	11.5-14.0	1.5-2.5	-	-	1.00	0.07
D	0.7-1.3	11.5-14.0	-	-	3.0-4.0	1.00	0.07
E-1	0.7-1.3	11.5-14.0	-	0.9-1.2	-	1.00	0.07

Table 1 shows the chemical composition of some commonly used austenitic manganese steel grades. The two main elements are C, and Mn. According to Subramanyam et al. (1990, pp. 1952-1956), the role of C in Hadfield steel is first and foremost to increase the rate of work hardening and the strength of the material. The optimal percentage of carbon to obtain a sufficiently high tensile strength is between, 1.05 and 1.35 %, this is due to the fact that it would become increasingly difficult to achieve an austenitic structure without the formation of carbides at grain boundaries. This is because the solubility of the alloy with a higher carbon content requires a lot of energy. Additionally, the effect of grain boundary carbides is negative in terms of ductility and strength.

The addition of Mn also contributes to the strength, namely ultimate strength of the material. By increasing the Mn content to approximately 12 %, the optimal ultimate strength is

obtained. It is at the same time the point at which the material reaches close to its maximum value for ductility.

The role of other commonly used trace elements such as Cr, Mo, nickel (Ni), silicon (Si) and phosphorus (P) is significant, especially for Cr, Mo and Ni. Both, Cr and Mo can be added to increase the yield strength provided the content of carbon is kept at a constant value of approximately 1.15 % Another benefit of adding Cr to the mixture is that the corrosion resistance improves. (Subramanyam et al. 1990, p. 1957.)

To increase the castability of Hadfield steel, Mo specifically can be used to supplement the toughness of the steel and to make it more resistant to being heated over and over during weld buildup or overlays. These are common occurrences in impact crushers for example. The last of the commonly utilized trace element is Ni and it is used for improving ductility but at the cost of a slight decrease in yield strength and abrasion resistance. (Subramanyam et al. 1990, pp. 1957-1958.)

Si and P content is largely related to production of the material as well as manufacturability. Si could potentially be used for increasing the yield strength of the steel. A Si content between 1-2 % could be beneficial for improved yield strength but very impractical because there exist other, more suitable elements for that purpose. As for P, a maximum content on 0.07 % is recommended to avoid low elongation at high temperatures. The result of low elongation at high temperatures can lead to tears and cracks in cast components. (Subramanyam et al. 1990, pp. 1956-1961.)

Furthermore, there are many more elements that can be added for obtaining specific properties. These elements include V, copper (Cu), bismuth (Bi), Ti and sulphur (S). (Subramanyam et al. 1990, pp. 1961-1962.)

3.1.2 Material Properties

As shown by the previous subchapter on the chemical composition of austenitic manganese steels, there exists multiple different variants each of which depend on the proportions of the trace elements and grain size in the material. Small changes to the chemical composition of Hadfield steel can result in wildly different material properties across the board.

To obtain a desirable state for the material such that it can be utilized in engineering applications, it typically requires heat treatment, namely solution annealing and quenching. The effect of heat treatment in combination with chemical composition is responsible for a wide range of properties. An example of the influence of the chemical composition and heat treatment can be observed in the tensile strength and elongation of austenitic manganese steel. According to Subramanyam et al. (1990, pp. 1973-1977), the difference in the tensile strength between fine and coarse grain can be as high as 30 % with fine grain possessing the higher value. Further, for a sufficiently well heat-treated specimen made of austenitic manganese steel with a medium grain size the tensile strength can vary between 620 MPa and 1035 MPa. As for elongation, the range can vary from as low as 13 % to as high as 67 %.

The yield strength of Hadfield steel is significantly lower than the tensile strength, by up to twice as low which signifies the materials exceptionally high work-hardening capacity. Typically, the yield strength is between 345 MPa and 415 MPa depending on the chemical composition which is on the boundary between mild and high strength steels, and the fatigue limit of Hadfield steel is also around 270 MPa depending on the testing conditions. Austenitic manganese steel and specifically Hadfield steel is however not known for its moderately high yield strength but rather its capacity to work-harden which is commonly taken advantage of in applications that require a high wear resistance. The capacity for Hadfield steel to work-harden is great. Depending on the composition, the surface hardness can harden from an initial state of 220 HV to above 900 HV. The capacity of austenitic manganese steels to work harden is attributed to three concepts, namely mechanical twinning, stacking fault formation, and dynamic strain aging (DSA). (Subramanyam et al. 1990, pp. 1977-1979.)

Karaman et al. (2000) investigated the role of mechanical twinning on work-hardening of single-crystal Hadfield steel, and they observed that twinning has a significant role in deformation of specimens where the crystal is under tensile or compressive stress. The method by which twinning contributes to work hardening is by introducing barriers that prevent the dislocation motion in a similar fashion to how grain boundaries do in polycrystal Hadfield steel. The formation of twin boundaries promotes the rate of strain hardening due to dislocation pileups resulting in a stronger material that is less prone for additional

dislocation along the same plane. The study also noted that the degree to which twinning occurs depends on the crystallographic grain orientation.

An intertwined mechanism that is a precondition to twinning that eventually contributes to work hardening is the stacking fault formation, and more specifically, the stacking fault energy (SFE), which is the driver of the aforementioned formation. According to Xiong et al. (2015), formation of twins could be observed in Hadfield steel once the strain rate exceeded 0.03, in comparison to comparable steel with high Mn content, the cause was attributed to the difference in SFE, which was slightly higher in Hadfield steel. However, compared to traditionally milder steels, the SFE of Hadfield steel is generally lower. The consequence of lower SFE is that the rate at which work hardening occurred was decreased due to lesser degree of twinning in Hadfield steel compared to austenitic steel with an even higher manganese content. Conversely, because Hadfield steel has a relatively low SFE in comparison to milder steels, mechanical twinning is more likely to occur.

Work-hardening factors affect the fatigue behaviour of austenitic stainless steels. In austenitic stainless steels, the influence of SFE is large because it contributes to work-hardening. However, findings by Moshtaghi and Safyari (2021) indicate that, while SFE influences the probability of stacking fault formation and crystallite size. Stacking fault probability does not affect the fatigue life of austenitic stainless steels. Rather, their fatigue resistance depends more on how dislocation arrangements develop during cyclic deformation.

The third contributing factor into work hardening of Hadfield steel is dynamic strain ageing (DSA) which is commonly attributed to the reorientation carbon in manganese-carbon couples. This effect can be helped further in an environment with increased temperature resulting in a larger energy that increases the movement of carbon atoms and prevents dislocation glide which in turn leads to strain hardening without the formation of twinning. Essentially, the dislocation motion gets momentarily stopped by obstacles. In order for the dislocation motion to proceed, a larger stress is needed which adds to strain hardening. (Canadinc et al. 2008.)

The influence of dislocation interaction on low-cycle fatigue has been investigated by Moshtaghi and Sato (2019), who studied the evolution of dislocation density in cyclically loaded ferritic and austenitic stainless steels. According to the findings, they observed a two-

stage process, where dislocation density increases quickly within the first cycles and then levels off after. A linear correlation was found between dislocation density and low-cycle fatigue life, meaning that in materials with a higher dislocation density, the fatigue life was shorter. This effect was more pronounced in austenitic stainless steel because of its higher work-hardening capacity and limited cross-slip capacity. The dislocation density was normalized with the maximum tensile work hardening which is how the linear relationship in low-cycle fatigue life was observed confirming that cyclic deformation and dislocation accumulation influence fatigue performance.

3.2 Fatigue

Fatigue as a concept refers to a mechanism whereby the application of a cyclic load can result in a component breaking after a sufficient number of load reversals has passed and it can occur with stresses far below the yield strength of the base material because over time, localized permanent change takes place in the base material. Fatigue as a mechanism consists of three distinct phases the first of which is crack initiation. Once a crack has formed to the component, it begins to propagate or increase in size until it grows so large that the component breaks because it is no longer able to withstand the applied stress. (Bathias & Pineau 2010, pp. 6-10.)

This subchapter provides an overview of fatigue as a phenomenon. It begins with a short introduction to its early history before examining the three main phases of fatigue and the different factors that influence fatigue strength. The objective of this subchapter is to build a foundation upon which the fatigue assessment of machine components made from Hadfield steel can be laid on by reviewing the underlying mechanisms of fatigue.

3.2.1 Brief Early History of Fatigue

Fatigue as a topic of research and a general area of study has been critical in the field mechanical engineering officially for close to 190 years. The first known experiment related to fatigue was published in 1837 by a German mining engineer Wilhelm Albert who built a machine for testing conveyor chains. The conveyor chains kept breaking after repeated use for reasons unknown at the time. However, while Wilhelm did conduct the first ever fatigue

test, the outcome of the tests was the invention of wire rope instead of insights into mechanics of materials. In fact, the term fatigue was not even used, rather it was implied (Schütz 1996, p. 264.)

The term “fatigue” was later brought up for the first time in 1854 in a publication by an English engineer named F. Braithwaite. Braithwaite’s publication noted, how multiple different types of equipment, such as water pumps, crankshafts, levers and cranes, had been broken due to fatigue failure. In addition to using the term fatigue, the paper discussed acceptable stresses for different machine components to avoid fatigue failure. In this time period, during a span of a decade, multiple railroad accidents occurred where the reason for failure could be attributed to fatigue. (Schütz 1996, pp. 2–3.)

A large breakthrough related to fatigue was made between the years from 1858 to 1860, when a German railway engineer named August Wöhler conducted fatigue tests on railway axles. The result of these tests was eventually used to formulate a method for estimating the durability of axles. Wöhler concluded in his publication that a component can break due to a cyclically applied load even if the magnitude of the applied stress is lower than the static strength of the base material. Wöhler even considered the effects of mean stress, stating that the effect of tensile mean stress on the component produces a lower fatigue life. The results of Wöhlers contribution to the study of fatigue eventually resulted in the creation of the stress–life curve (S-N curve) but while the S-N curve was first plotted by a contemporary of Wöhler, the S-N curve is commonly known to this day by another name, Wöhler curve and it is still used extensively to estimate the fatigue life of components made from different materials. (Schütz 1996, pp. 3–4.)

3.2.2 Crack Formation

The first phase of fatigue is the formation of a crack on the surface of the material. According to Schijve (2009, pp. 14-15), studies into the initiation phase of fatigue have revealed that the process through which fatigue cracks form begins at a microscopic level. It is argued that microcracks form almost from the beginning when a cyclic load is applied to a component, assuming the magnitude of the applied load exceeds the fatigue limit of the material. It is still a commonly held assumption that loads with a magnitude below the fatigue limit of the

material do not result in failure due to fatigue. However, the previous assumption is still contested.

The formation of fatigue cracks is largely the result of cyclic slip which refers to plastic deformation on a microscale occurring locally on the free surface of the component as a result of the applied stress. For dislocations to move along the slip planes, a cyclic shear stress is required. Since the material is inhomogeneous on a microscale, the effect is disproportionate, wherein a localised area on the surface of the component is more susceptible to the slip occurring. The localised area is commonly a site with a discontinuity resulting in a concentration of stress. As a slip occurs, a slip step will form, which subsequently exposes a new surface to the surrounding conditions, and the process repeats itself. (Schijve 2009, pp. 15-16.)

If the applied load is also increased, the slip band will strain harden, making it more resistant to further dislocation in the same direction. Upon unloading, the strain-hardened slip bands experience slip in the opposite direction. However, due to strain hardening, the initial slip plane can become less prone to additional slip, thus making the adjacent planes along the same direction more likely to experience slip. This potential change to an adjacent slip plane during cyclic loading typically leads to intrusions, which are the very microcracks that subsequently become macro cracks. (Schijve 2009, pp. 16-18.)

3.2.3 Crack Growth

Once a microcrack has formed on the surface of the component, a localised change in the general stress state occurs where the tip of the crack acts as a stress raiser. As the size of the crack grows beyond the size of a single grain, adjacent grains and slip planes can become alternative paths for crack growth. The probability of the path to deviate becomes increasingly likely due to the fact that dislocation motion along a specific slip plane is unlikely to keep repeating. Rather, the crack will change its direction to where it grows perpendicular to the applied load. (Schijve 2009, pp. 18-19.)

According to Schijve (2009, pp. 19-21), the growth of microcracks can be impeded by obstacles. Typically, the growth rate of cracks slows when the crack reaches one. One such obstacle can be the boundary between adjacent cracks. The reason for the reduction of the

growth rate can be explained by the fact that the slip plane in the adjacent grain is unlikely to be aligned with the plane in the original grain which means that the crack has to find an alternative route to continue. Although the speed at which the crack grows can be impeded for a duration, the global direction of crack growth remains relatively unchanged meaning that the direction of the crack growth does not change randomly at each boundary but rather continues to grow driven by the stress intensity at the tip of the crack. The concept of stress intensity shall be covered in depth in a later chapter concerning fracture mechanics.

3.2.4 Fracture

The third and final phase of fatigue is the failure of the component or structure under consideration. The final fracture occurs once the fatigue crack has grown so large such that the remaining amount of material is incapable of withstanding the applied load. The process through which final failure occurs can be either ductile, brittle or a combination of the two depending on the material and the conditions that the part is subjected to. (Wulpi & Miller 2013, p. 121.)

3.2.5 Fatigue Strength

The fatigue strength of a machine component or a test specimen is not simply a question of the material being tested but rather involves many variables, each of which contributes to the fatigue performance of the component. As stated in a previous chapter on Hadfield steel, their fatigue strength is commonly around 270 MPa, but depending on the testing setup and specific chemical composition, the fatigue strength can vary. The critical factors that influence the fatigue performance of Hadfield steel include microstructure of the material, size of the component, surface finish, frequency of the applied load, mean- and residual stresses, environmental considerations such as corrosion and the applied load type.

Effect of Microstructure

The work by Stephens et al. (2001, p. 79) covers the first four aspects, namely microstructure, size, surface finish and frequency. The role of microstructure in assessing

the fatigue performance of a component is relatively large. The effect of grain size on the tensile strength of Hadfield steel can be as large as 30 % favouring small grain size over large grain size. This observation also coincides with findings from other materials as well, albeit to different degrees depending on the specific alloy.

The reason why smaller grain size is commonly more beneficial as opposed to large grain size, especially in terms of fatigue performance, is that the presence of a large number of grain boundaries has a tendency to hinder the growth of fatigue cracks by creating barriers at closer intervals where the rate of crack growth slows down significantly and even stops for a while. Another factor to consider related to microstructure is grain orientation and impurities such as porosity and inclusions. If the applied load is in the same direction as the grains, the fatigue strength is also much improved. As for impurities in the metal, the existence of inclusions and pores typically lowers the fatigue performance as they provide additional locations for fatigue cracks to form. These localized imperfections result in stress concentrations that make it advantageous for the cracks to form. (Stephens et al. 2001, pp. 79-80.)

Effect of Size

Increasing the size of the component beyond a certain point has a negative effect on its fatigue strength. The reason is twofold, the first of which is related to the applied load. If the component is subjected to a uniform bending about its neutral axis, resulting in a compressive stress on the top and tension at the bottom fibre, the stress gradient is different between a thinner and a thicker component. In the thicker component, the average stress approaching the extreme fibres of the cross-section is larger because the stress gradient is smaller. The size effect is therefore slightly larger in cases where bending governs but it also exists in cases where the applied load is uniform tension. For uniform tension, the reason for why the fatigue strength is lower is due to discontinuities in the material. This is because for larger specimens, the increased surface area and volume have more room for discontinuities, whereas in a smaller specimen, there is less room. Consequently, a smaller component possesses in improved fatigue resistance all else being equal. If the two specimens are made from the same alloy, the likelihood of discontinuities and impurities is higher in the larger component. (Stephens et al. 2001, p. 80.)

Effect of Surface Finish

As the initial phase of fatigue is largely a surface phenomenon, the role of surface finish is bound to have an influence on the fatigue strength of the component. According to Milella (2024, pp. 145-148), surface finish refers to how smooth or rough the surface of the material is as measured by common roughness parameters. The reason for why the quality of surface finish influences the fatigue strength of the component is that the more discontinuities there are, the more places exist for cracks to form. This happens because these small discontinuities create stress concentrations locally and then quickly thereafter become the very locations for micro cracks to grow due to the locally increased stress state.

There also appears to be a relationship between the tensile strength of the base material and the surface finish. More specifically, the relationship appears to be beneficial as it relates to the fatigue strength of steels with excellent strain hardening capacity. Although the reason behind it remains unclear. However, it is argued that the yield strength of the material acts as a preventative measure against slip at the beginning but as soon as slip occurs, the degree to which it continues is tied to the ability of the material to harden. (Milella 2024, pp. 150-152.) The exceptional strain-hardening capacity of Hadfield steel may be one of the reasons behind the relatively high fatigue strength.

Effect of Frequency

The role of frequency in fatigue strength is at best negligible and at worst, inconclusive. According to Stephens et al. (2001, pp. 82-83), if environmental influences such as corrosion and temperature can be controlled, the effect of frequency can be isolated. For example, if a larger test specimen is subjected to a cyclic axial load at a high frequency, the temperature of the specimen can quickly rise because of internal hysteresis damping. For large specimens, the temperature effect will also be multiplied thus potentially falsifying the effect of frequency. Fatigue tests have also shown that the effect of frequency can be both beneficial and negative in terms of fatigue life depending on the material under consideration The increase in fatigue life at frequencies below 200 Hz has been observed to be up to 10 %, at above 1000 Hz, the effect can be even higher, even up to 2.6 times. However, the increased temperature due to a higher frequency makes the underlying influence of frequency hard to isolate and estimate.

Effect of Mean and Residual Stress

With regard to fatigue of base material, mean stress can either significantly reduce or increase the fatigue performance of machinery components depending on the type of mean stress. There exists two types, namely tensile mean stress and compressive mean stress with tensile mean stress being the one that contributes negatively to fatigue life. The negative effect of mean stress is the result of accumulation of strain or cyclic creep. The accumulation of strain directly contributes to crack growth by way of increasing the amount of plastic deformation. Tensile stress commonly also attempts to open the fatigue crack at every cycle whereas in the case of compressive mean stress, the effect is opposite. With compressive mean stress, at every load cycle, the fatigue crack closes which in turn slows down the growth of the crack and prolongs the fatigue life of the component. (Stephens et al. 2001, pp. 74-77.)

A similar observation has also been made with regard to the effect of residual stresses wherein a presence of compressive residual stress, the fatigue life of a specimen is higher as opposed to one where the residual stress state is in form of tensile stress. According to Schijve (2009, pp. 89-98), residual stresses refer to internal stresses. That is to say that their existence does not depend solely on the applied load but rather they can be the result of manufacturing processes. Residual stresses have an effect on the level of mean stress, in case of tensile residual stress, they in essence increase the level on mean stress. However, unlike mean stress, the residual stress state can be removed and even altered. To remove residual stresses from a component, one approach is to heat up the component. To change tensile residual stress into compressive, shot peening is a viable method where the surface of the component is modified through small plastic deformation which introduces a compressive residual stress near the top layer.

Effect of Environment

Environmental considerations such as contact with elements that corrode metal are also one mechanism by which the fatigue strength of steel is reduced. According to Milella (2024, pp. 161-164), the formation of particles due to corrosion on the surface of the component results in a situation which is advantageous for a fatigue crack to form. Once the initiation

phase of fatigue has concluded, the effect of corrosion can also be observed in the growth phase in the form of an increased crack growth rate.

Effect of Load Type

Lastly, the effect of applied load type on fatigue strength will be considered. There are four primary loading types, axial, bending, torsion as well as shear loads. The primary types can be further divided into different categories. The difference in fatigue strength between axial loading and cyclic or rotating bending is approximately 5 to 10 % with axial loading possessing a lower fatigue limit. This is due to the decrease in stress for the component subject to bending where the stress approaches zero towards the neutral axis, for tension, the stress is uniformly distributed throughout the whole cross-section. The shape of the cross-section is also of importance. For hollow round sections, the previously mentioned holds true but for flat sections, the differences are only due to the effect of the stress gradient. In the case of rotating bending, the stress state is similar to the cyclic tension because of the rotation, but the presence of stress gradient is still slightly beneficial compared to cyclic tensile stress. (Milella 2024, pp. 193-196.)

While on the surface, torsion appears to mimic the rotating bending, Milella (2024, pp. 196-200) argues that since the resulting shear stress due to torsion is significantly different from the other two load types, the stress state in the material also changes to biaxial. A change to biaxial stress state also shows up in an increase in the magnitude of stresses by a factor of up to 2 compared to the equivalent applied bending moment. The effect in this instance leads to an increase of 1.73 in fatigue strength in favour of rotating bending. The effect on the fatigue limit also depends on the material used; for cast iron, the fatigue limit between tension and torsion can be as high as 0.9, but for titanium, the limit can be as low as 0.48.

Before concluding this subchapter, the effect of notches on fatigue strength shall be mentioned but briefly. Notches in general are discontinuities that result in a locally increased stress, making these discontinuities an ideal place for fatigue cracks to nucleate and grow to failure. As the influence of notches on fatigue strength is large, a separate subchapter will be dedicated to it.

In closing, fatigue strength is a complicated concept that involves multiple factors. Here, microstructure, size, surface finish, frequency, mean- and residual stress, and load type were

considered, each of which contributes to varying degrees to the fatigue strength of the material. Since the role of the previously considered factors is of great importance, effort must be paid to them as they relate to the fatigue strength of Hadfield steel.

3.3 Stress – Life Approach

The stress-life (S-N) approach is a widely used method where a relationship between the applied stress and the number of cycles to failure can be used to describe how a component responds to cyclic loading and to determine the number of cycles a component can withstand before breaking. The S-N approach is originally built on the work by A. Wöhler, and it makes for an excellent tool for assessing the fatigue life of a given material or component. The S-N method is especially well-suited for evaluating high-cycle fatigue where the role of plastic deformation is small. A small amount of plastic deformation as a result of cyclic loading is commonly associated with smaller stresses, thereby necessitating a large number of cycles before the component fails due to fatigue. (Lee et al. 2005, pp. 103-104.)

3.3.1 Definitions

To understand the S-N approach, some commonly held definitions of the basic concepts are introduced, beginning with a cyclic stress diagram. A cyclic stress diagram displays the magnitude of the applied stress over a certain number of cycles or a time span. An example of a constant amplitude cyclic stress diagram is presented in Figure 1.

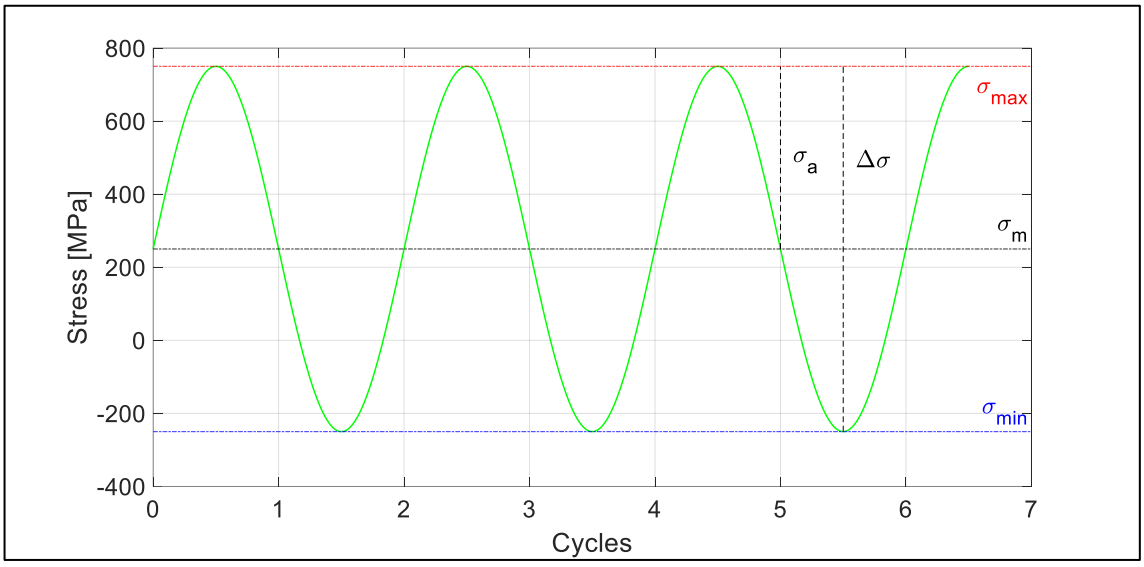

Figure 1. Cyclic stress diagram.

The cyclic stress diagram shown by Figure 1 displays some important concepts, namely maximum, minimum and mean stress as well as the stress range, stress amplitude and stress ratio. The terms maximum and minimum stress are fairly straightforward in so far as they describe the maximum and minimum applied or experienced stress over the observable span of time or over a certain number of cycles. For the remaining terms, more rigorous definitions are needed.

Beginning with mean stress, mean stress refers to the average stress over a specific span. From Figure 1, the mean stress is represented by the line dividing the stress cycle in half (Lee et al. 2005, p. 104). The definition of the mean stress can be expressed as follows:

$$\sigma_m = \frac{\sigma_{max} + \sigma_{min}}{2} \quad (1)$$

Where σ_{max} is the maximum stress and σ_{min} is the minimum stress. The mean stress can therefore be obtained by dividing the sum of the maximum and minimum stress by two.

Next up the stress range, and the stress amplitude. The stress range is defined as the difference between the minimum and the maximum applied stress whereas the stress

amplitude is the stress range divided by two (Lee et al. 2005, p. 104). Stress range and stress amplitude are formulated as follows:

$$\Delta\sigma = \sigma_{max} - \sigma_{min} \tag{2}$$

$$\sigma_a = \frac{\Delta\sigma}{2} = \frac{\sigma_{max} - \sigma_{min}}{2} \tag{3}$$

Both the stress range and the stress amplitude can also be seen from Figure 1. Stress range is marked with a black line that goes from the lowest valley to the highest peak and stress amplitude is the black line from the mean stress to the maximum stress.

Lastly the stress ratio which tells the difference between the minimum and maximum stress as a factor with a magnitude in between one and minus infinity (Lee et al. 2005, p. 105). The stress ratio can be written as:

$$R = \frac{\sigma_{min}}{\sigma_{max}} \tag{4}$$

With the basic definitions provided, their role in assessing the fatigue life of a component can be established, beginning with the S-N curve.

3.3.2 S-N Curve

S-N curve or otherwise known as the Wöhler curve is a method for presenting the results of a fatigue test by fitting a line through a series of data points. The data points correspond to the number of cycles it took to break the test specimen given a specific stress amplitude or stress range. (Pook 2007, pp. 15-18.) An example of an S-N curve can be seen from Figure 2.

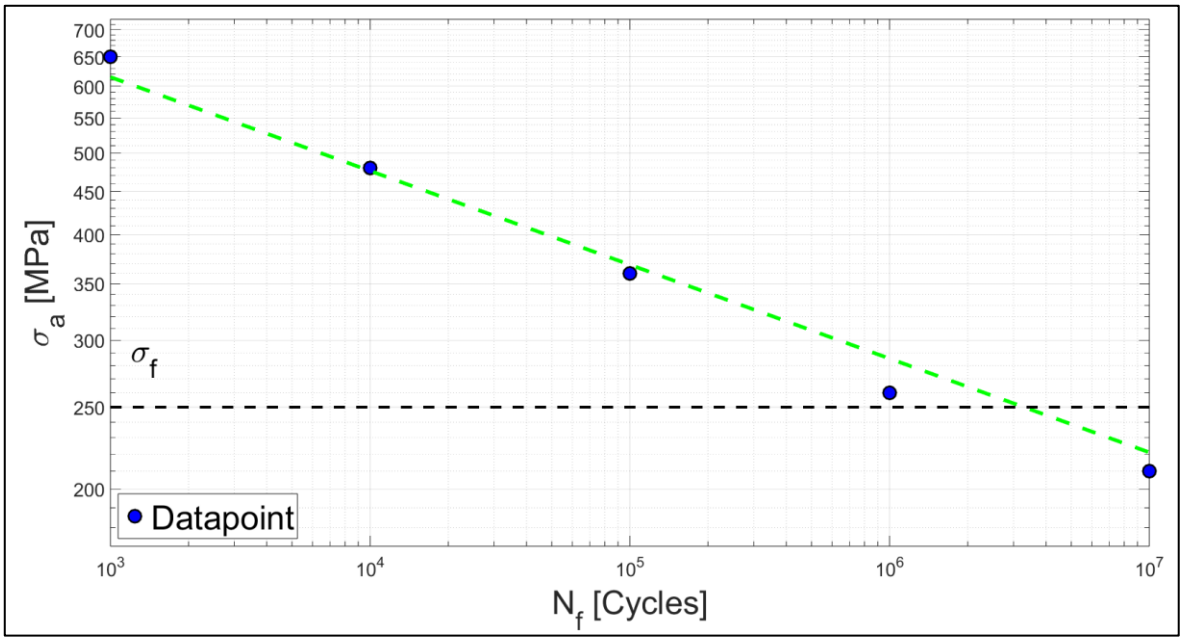

Figure 2. S-N Curve

Figure 2 contains an S-N curve, which is a fitted line based on the test data. The test data in this instance is represented by the blue markers. A horizontal dashed line indicates the fatigue limit which is denoted by σ_f that corresponds to a stress amplitude of 250 MPa meaning that a stress amplitude lower than that does not cause the fatigue crack to grow, and the component can be thought to have an infinite life if the stress amplitude does exceed 250 MPa. The fatigue limit is reached at approximately 2,000,000 cycles in this imaginary example.

An S-N curve similar to the one shown by Figure 2 can be plotted using Basquin's equation and by setting the X and Y-axes to logarithmic scale (Milella 2024, p. 316). Basquin's equation can be defined as:

$$\sigma_a = \sigma_f' (N_f)^b \tag{5}$$

Where σ_f' is the fatigue strength coefficient. N_f corresponds to the number of cycles, and b is the fatigue strength exponent or the slope of the inclined portion of the S-N curve.

Given the large influence of mean stress on the fatigue life of a component, several assessment methods have been developed for this purpose, two of which are presented next.

3.3.3 Stress-Based Assessment Methods

In stress-based fatigue analysis, five different methods are commonly used to account for the effect of mean stress. These assessment methods differ from each other mostly by how they account for mean stress in the determination of fatigue life. The five different methods include modified Goodman, Gerber parabola, Morrow, Smith-Watson-Topper (SWT), and Walker method. The modified Goodman generally overestimates the influence of mean stress resulting in an excessively large margin of safety. The Gerber parabola has the opposite issue as modified Goodman insofar as it results in an underestimation of the effect of mean stress especially with ductile materials. (Dowling 2013, pp. 454-455.)

Morrow was able to discover a solution to the problem posed by the Gerber parabola for ductile materials by utilizing the corrected true fracture strength of a material. However, the corrected true fracture strength necessitates a separate tensile test which makes the method inconvenient in practical applications in comparison to alternative approaches. Out of the five stress-based assessment methods, two stand out as both popular and reasonably accurate, namely the SWT, and Walker method. These two methods are relatively similar to each other in that SWT closely resembles the Walker method assuming a specific value for the material constant. (Dowling 2013, pp. 455-456.)

SWT in its stress-based version may be denoted as:

$$\sqrt{\sigma_{max}\sigma_a} = \sigma_f'(2N_f)^b \tag{6}$$

Based on Equation 6, SWT assumes that fatigue failure occurs only in the presence of tensile stress, meaning that compressive stress would result in an infinite fatigue life. This follows from the fact that if the maximum stress σ_{max} is less than or equal to 0 MPa, the number of cycles is either infinite or undefined. According to Andersson (2021, p. 32), the advantage of using SWT is that it does not depend on any material specific properties unlike the Walker method.

The Walker method, while being similar to SWT differs a fair bit in terms of accuracy by a material property that is used in conjunction with it. The Walker method is represented as:

$$\sqrt{\sigma_{max}^{1-\gamma}\sigma_a^{\gamma}} = \sigma_f'(2N_f)^b \quad (7)$$

Where γ is the material parameter. The Walker method is potentially more accurate compared to the other methods provided data is available for the material being analysed. If data is unavailable, the material constant can be obtained by conducting fatigue tests on several specimens and then performing a linear regression analysis based on the test data to obtain the value of the material parameter. (Dowling 2013, pp. 516-517.)

3.4 Strain – Life Approach

Fatigue assessment methods based on strain are more focused on the first phase of fatigue or the fatigue crack initiation. This is because the first phase of fatigue is driven by plastic deformation. Therefore, stresses beyond the yield strength of the material are no longer pertinent, instead strain becomes the relevant factor. Fatigue assessment methods based on strain are especially suitable for low-cycle fatigue. This is due to the presence of larger stresses that lead to permanent deformation, and permanent deformation cannot be described accurately by using linear elastic stress state because the relationship between deformation and stress post-yielding is nonlinear. The relationship between fatigue life and the applied stress therefore results in a mismatch because stress-based methods do not account for changes in the material such as strain-hardening. (Milella 2024, pp. 355-356.)

While the strain-based approach works exceptionally well for low-cycle fatigue analysis, it is also suitable for fatigue analysis of moderate and even high-cycle regime. The difference is that at higher cycles, the assessment methods comprise largely of the elastic regime which is to say that for cases concerning high cycle fatigue, the approach is reduced to a form, where the total strain can be evaluated with a relationship resembling the one used for stress-life approach because the plastic strain component becomes non-existent and the relationship is reduced to a linear model. (Milella 2024, pp. 356-362.)

3.4.1 ε – N Curve

The strain-life curve is equivalent to the S-N curve shown in the previous subchapter by Figure 2. While Basquin discovered a geometric relationship between the elastic strain component and number of cycles in the early 1900's, it wasn't until the middle of the century when both Manson and Coffin at approximately same time but independent of each other arrived at an expression that revealed a relationship between the plastic strain component and number of cycles to failure. This discovery is known today as the Manson-Coffin relationship. (Milella 2024, pp. 360-361.) It can be expressed as follows:

$$\varepsilon_p = \frac{\Delta\varepsilon_p}{2} = \varepsilon_f'(N_f)^c \tag{8}$$

Where $\frac{\Delta\varepsilon_p}{2}$ is the plastic strain amplitude, ε_f' is the fatigue ductility coefficient and c is the fatigue ductility exponent. Similarly to Basquin's equation, Equation 5, Manson-Coffin relationship becomes a straight line if plotted using a logarithmic scale on both axes.

The contribution by Manson and Coffin incorporated with Basquin's relationship made it possible to generate a complete plot combining both elastic and plastic strain components into a single curve known as the ε-N curve (Milella 2024, pp. 361-362). The complete expression representing the total strain is otherwise known as the Coffin-Manson-Basquin relationship and it is given by:

$$\varepsilon_a = \frac{\sigma_f'}{E}(N_f)^b + \varepsilon_f'(N_f)^c \tag{9}$$

Where ε_a is the strain amplitude, E is Young's modulus. The second part of the right-hand side represents the plastic component shown previously by Equation 8, and the first part is the elastic component. An example of an ε-N curve is presented in Figure 3.

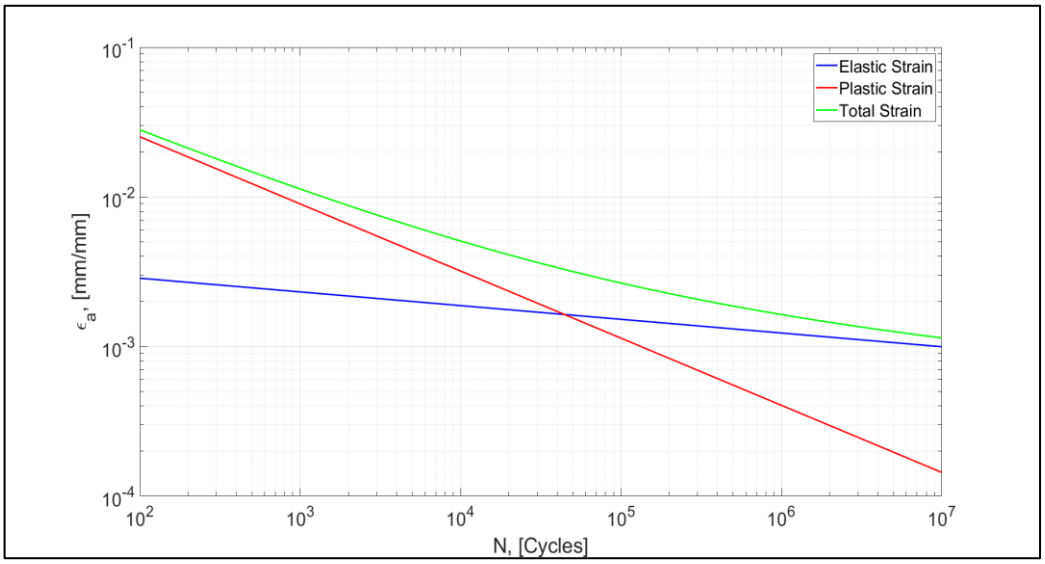

Figure 3. Total strain, Manson-Coffin-Basquin

Figure 3 contains three separate curves, one marked with a blue colour representing the elastic strain component, and another marked with red colour that represents the plastic strain component. The total strain is plotted in green colour and is the summation of the two separate components. Figure 3 illustrates the relative contributions of each component. The elastic strain component has a smaller slope making it more consequential for high-cycle regime whereas the plastic strain component contributes significantly initially to the total strain and then becomes trivial as the number of cycles increases.

3.4.2 Strain-Based Assessment Methods

Similarly to the stress-based approach, strain-life curves are originally based on zero mean stress. Therefore, in practical applications where a mean stress is present, strain-life curves are modified to account for the effect of mean stress. The role of mean stress depending on its magnitude and whether it is compressive or tensile, can be either beneficial or alternatively reduce the fatigue life of the component. (Lee et al. 2005, p. 208.)

According to Dowling (2013, p. 761), there are four commonly utilized strain-life methods for estimating the fatigue life of a component. The four main approaches are by Morrow, SWT and Walker. There exist two variants with Morrow the first of which is the original Morrow mean stress equation. Morrows' original approach highlights that the effect of mean

stress has been accounted by both the elastic and plastic strain components. Morrows' original approach takes the form:

$$\varepsilon_a = \frac{\sigma_f'}{E}\left(1 - \frac{\sigma_m}{\sigma_f'}\right)(2N_f)^b + \varepsilon_f'\left(1 - \frac{\sigma_m}{\sigma_f'}\right)^{\frac{c}{b}}(2N_f)^c \tag{10}$$

Morrows original mean stress equation is essentially the Coffin-Manson-Basquin relationship that has been modified to account the effect of mean stress by changing the intercept constants. The mean stress is accounted for by two additions. First, by adjusting the stress amplitude and then correcting the fatigue life for mean stress as expressed by the following:

$$\sigma_{ar} = \frac{\sigma_a}{1 - \frac{\sigma_m}{\sigma_f'}} \tag{11a}$$

$$N_f = N_{mi}^*\left(1 - \frac{\sigma_m}{\sigma_f'}\right)^{-\frac{1}{b}} \tag{11b}$$

Where σ_{ar} is the equivalent completely reversed stress amplitude that enables the transformation of a cyclic load with mean stress to an equivalent load that behaves like a fully reversed cycle. N_{mi}^* is the corrected fatigue life using an intercept constant from stress-life approach. According to Dowling (2013, pp. 762-763), Morrows' approach to include the effect of mean stress into both elastic and plastic parts overestimates the role of mean stress in the plastic region. As a solution to this issue Morrow suggested an alternative approach entitled the modified Morrow approach, which takes the form:

$$\varepsilon_a = \frac{\sigma_f'}{E}\left(1 - \frac{\sigma_m}{\sigma_f'}\right)(2N_f)^b + \varepsilon_f'(2N_f)^c \tag{12}$$

The modified Morrow approach neglects the mean stress correction entirely from the plastic strain component. The overestimation of mean stress in the plastic component occurs

because in the low cycle regime, plastic deformation induces a state of stress relaxation where an initial mean stress tends to approach zero as time passes. For moderate to long lives, the effect of mean stress is large in the elastic range hence only the elastic component is modified.

The third strain-based approach is by Smith, Watson and Topper where the product of the maximum tensile stress and the strain amplitude is used to estimate the amount of damage a specific cycle constitutes out of the entire fatigue life for fully reversed loading. SWT approach is described by:

$$\sigma_{max}\varepsilon_a = \frac{(\sigma_f')^2}{E}(2N_f)^{2b} + \sigma_f'\varepsilon_f'(2N_f)^{b+c} \tag{13}$$

Similarly to its stress-based counterpart, the strain-based method requires a greater than zero tensile stress to be present for fatigue damage to occur. The SWT parameter on the right-hand side of Equation 13 can be further expanded as follows, or alternatively redefined in the following ways:

$$\sigma_{max}\varepsilon_a = (\sigma_m + \sigma_a)\varepsilon_a \tag{14a}$$

$$\sigma_{max}\varepsilon_a = \sigma_{ar}\varepsilon_{ar} \tag{14b}$$

Where ε_{ar} is completely reversed strain amplitude. The SWT parameter is equivalent to the product of a fully reversed strain and stress amplitude. In the first expression 14a, σ_{max} component in the SWT parameter consists of two variables, mean stress and the stress amplitude. The effect of mean stress is therefore included in the SWT parameter itself.

The fourth strain-based approach is the Walker method which according to Dowling (2013, p. 765) agrees reasonably with SWT if the material parameter γ is assigned a value of 0.5. Other than this special case, the Walker method is a completely separate assessment method. The Walker method takes the form of:

$$\varepsilon_a = \frac{\sigma_f'}{E}\left(\frac{1\text{-}R}{2}\right)^{\gamma}(2N_f)^b + \varepsilon_f'\left(\frac{1\text{-}R}{2}\right)^{\frac{c(1-\gamma)}{b}}(2N_f)^c \quad (15)$$

However, like Walkers' stress-based counterpart, the strain-based version also requires that the material parameter be first obtained experimentally, which can present issues in fatigue assessment if data is not readily available. If either data can be made available or a test can be conducted to obtain the material parameter, the Walker method is the most accurate out of the strain-based options considered heretofore for steels, aluminium and titanium. The most versatile method is, in any case, the SWT due to its simplicity and ease of use as well as its capability for estimating a large number of different materials with acceptable accuracy. (Dowling 2013, p. 765.)

3.5 Fracture Mechanics

The study of fracture mechanics focuses on assessing how a pre-existing crack in a component or structure develops under load and affects the durability of components. Modern manufacturing techniques are still unable to eliminate the formation of cracks in components. Initial defects like small cracks have a negative influence on the structural durability, and depending on the application, they need to be considered to ensure that the design is up to specifications. According to Maiti (2015, pp. 1-2), the field of fracture mechanics began early 1900s by A. A. Griffith but it was not until the middle of the century that his theories were used and improved upon to solve problems related to fatigue that could not be solved by other traditional methods, specifically problems related to brittle fracture.

The field of fracture mechanics is vast, and in this case, the topic of fracture mechanics will only focus on linear elastic fracture mechanics, its key concepts, and application to fatigue assessment.

3.5.1 Crack Opening Modes

A fatigue crack can be represented as two surfaces that are joined together forming a sharp edge. When a cyclic load is applied to the component, the fatigue crack begins to grow.

There is a total of three distinct crack opening modes which refers to the relative motion of the two surfaces due to the direction of the applied load. The three separate modes or a combination thereof can be used to determine the mode of fracture in a given component. (Sun 2011, pp. 25-26.) The three crack opening modes are presented in Figure 4.

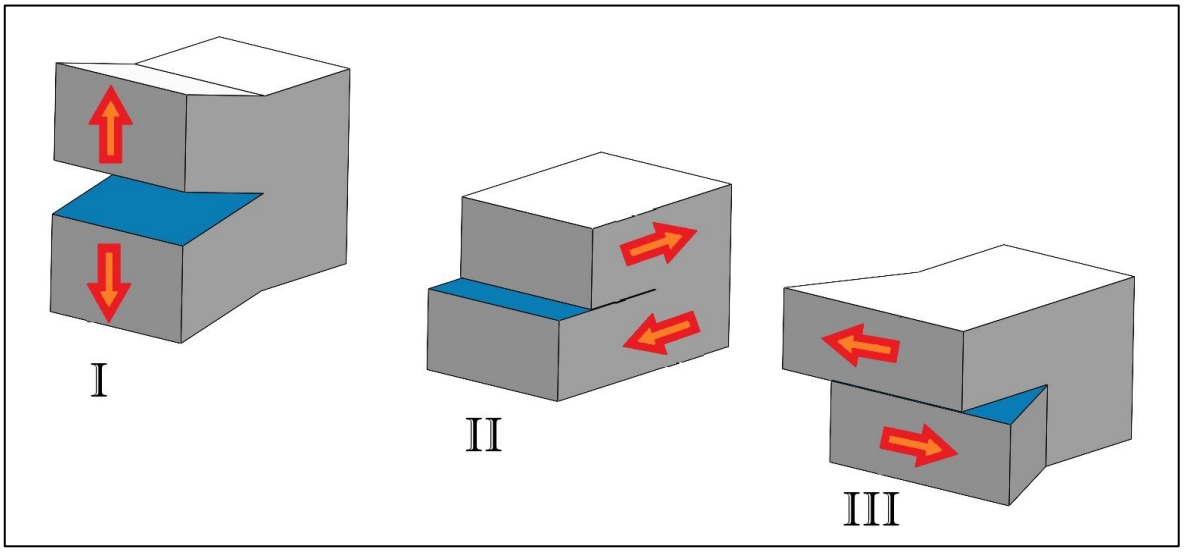

Figure 4. Crack opening modes

Starting from the left in Figure 4, the first crack opening mode is the opening mode in which the two separate surfaces are being pulled apart (Sun 2011, pp. 25-26). The stress corresponding to the crack front or the sharp tip is then expressed as:

$$\sigma_{yy}=\frac{K_I}{\sqrt{2\pi x}}+O\left(\sqrt{x}\right),\ \ \sigma_{xy}=\sigma_{yz}=0 \tag{16}$$

Where K_I is the stress intensity factor for the opening mode. O refers to higher order terms. The second opening mode is called the sliding mode, where the two surfaces slide in opposite directions but along the same plane. (Sun 2011, pp. 25-26.) The stress in the crack front for opening mode two is defined by:

$$\sigma_{xy}=\frac{K_{II}}{\sqrt{2\pi x}}+O\left(\sqrt{x}\right),\ \sigma_{yy}=\sigma_{yz}=0 \tag{17}$$

Where K_{II} is the stress intensity factor for the sliding mode. The final opening mode is known as the tearing mode where the two surfaces move along the same plane as the crack but in opposite directions. (Sun 2011, pp. 25-26.) The stress at the crack front for mode three is denoted as:

$$\sigma_{yz}=\frac{K_{III}}{\sqrt{2\pi x}}+O\left(\sqrt{x}\right),\ \sigma_{yy}=\sigma_{xy}=0 \tag{18}$$

Where K_{III} is the stress intensity factor for the tearing mode. Based on Equations 16-18, the three opening modes reveal a stress singularity at the tip of the crack. Singularity at the crack tip means that the stress at the tip of the crack reaches infinity in theory due to an infinitely sharp crack tip. (Sun 2011, pp. 26-27.)

According to Anderson (2005, pp. 61-62), the reason why in practice, the tip of the crack does not experience infinite stress like theory suggests is that in practice, a crack does not possess an infinitely sharp tip, but it is rounded to different degrees. Due to the rounded edge, the stresses at the tip of the crack are finite and possible to approximate through analytical and numerical approaches. The chosen approach depends on the degree of plasticization. The degree to which plasticization occurs at the tip of the crack determines whether LEFM is applicable or not for estimating the stress state. Since some form of plastic deformation does occur, there exist methods that are able to account for the plastic deformation and the resulting strain hardening while enabling the use of LEFM.

3.5.2 Stress Intensity Factor, Energy Release Rate and Fracture Toughness

As alluded to in the subchapter on fatigue, the driving force at the tip of the crack, or the reason for why the crack keeps growing, is because of the stress intensity factor (SIF). According to Anderson (2005, pp. 43-45), SIF is used to describe the stresses, strains and

displacements at the tip of the crack, making it one of the key concepts in the field of fracture mechanics.

The SIF is a quantity that can be obtained analytically for very simple cases and through experimentation for complex problems. For mode one opening, an analytical approach can be utilized for a through crack in in infinite plate assuming a proportional response wherein the stress at the tip of the crack responds linearly to the applied stress. (Anderson 2005, p. 46.) In a simple analytical case, the SIF for mode one can be described as:

$$K_I = \sigma\sqrt{\pi a} \tag{19}$$

Where σ is the applied stress and a is the initial crack size. The magnitude of the SIF depends on the geometry of the crack and even the specimen. For example, in a semi-infinite plate with an edge crack, the SIF is 12 % larger than in the previously mentioned case shown by Equation 19. (Anderson 2005, p. 46.)

While the SIF is the driving force of crack growth, the driver is another critical concept in fracture mechanics. The driver in this instance refers to the energy release rate or the energy that drives the growth of cracks. The expression for energy release rate is expressed as:

$$G = -\frac{d\Pi}{dA} \tag{20}$$

Where Π is the potential energy in an elastic body and A is the area of the crack. Equation 20 states that the rate of change of potential energy depends on the area of the crack. (Anderson 2005, pp. 34-35.)

Anderson (2005, pp. 58-60) states that together the aforementioned concepts of SIF and energy release rate are used to obtain a general relationship for plane stress and plane strain that can be applicable to all opening modes acting simultaneously or each of them separately. The relationship for plane strain for all the modes acting at the same time can be written as:

$$G=\frac{K_I^2}{E'}+\frac{K_{II}^2}{E'}+\frac{K_{III}^2}{2\mu} \tag{21}$$

Where E' is a term used to define both plane stress and plane strain conditions by utilizing Young's modulus for plane stress and a relationship between Young's modulus and Poisson's ratio for plane strain. μ refers to the shear modulus.

Another important quantity in fracture mechanics is the concept of fracture toughness. According to (Gdoutos 2020, p. 13), fracture toughness refers to the degree to which the base material is able to withstand breaking. The value for fracture toughness can be associated with the strength of the material using an inverse relation where for steels with larger yield strength, the value of fracture toughness is lower. Consequently, if the size of the initial crack in a high strength steel is larger, the likelihood of brittle fracture increases.

3.5.3 Fracture Mechanics as a Tool for Fatigue Assessment

While fracture mechanics deals mostly with the growth phase of cracks, it can also be used for fatigue assessment. Each of the three phases of fatigue can be modelled by using the crack growth rate and stress intensity factor range. (Zehnder 2012, pp. 71-72.) Crack growth rate as a function if stress intensity factor range results in a graph like the one presented in Figure 5.

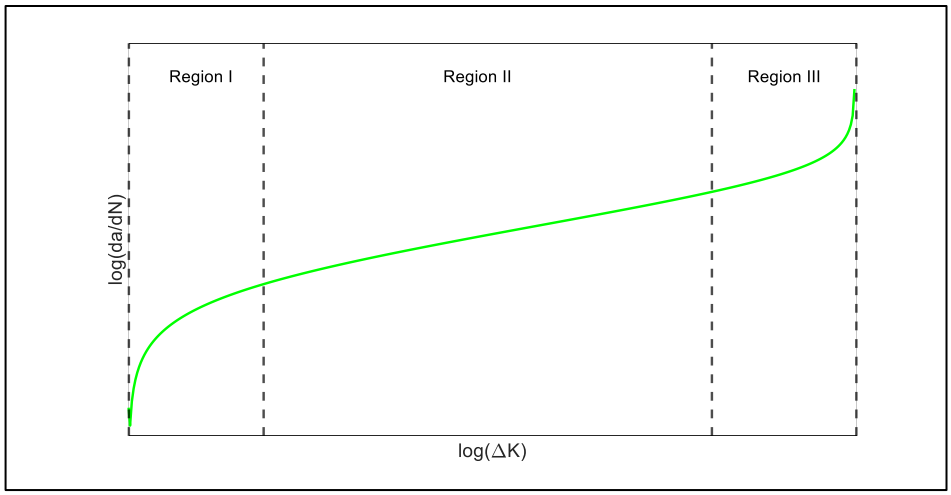

Figure 5. Sigmoidal Curve

Figure 5 depicts what is known as a sigmoidal curve. The curve can be divided into three distinct regions each of which correspond to a specific phase of fatigue. Beginning with region one on the left. The first region corresponds to the initiation phase of fatigue or crack initiation and the sigmoidal curve states that if the stress intensity factor range is sufficiently small, there will not be any noticeable crack growth. (Zehnder 2012, p. 71.)

The largest part of fatigue is often taken up by the second phase or crack propagation and that is what region two highlights. Arguably, the middle region is the most important out of the three because that is where most of the time will be spent for ductile materials. The second region is of such great importance that many different approaches have been developed to model it. The purpose of these different approaches is to generate a method for estimating the fatigue life of any given component. One of the most notable of these methods is by Paris and Erdogan otherwise known as the Paris law. (Zehnder 2012, p. 72.) Paris law will be introduced in more detail in the next subchapter.

The third and last region represents the final failure of the component where the stress intensity factor exceeds the value of fracture toughness of the base material, and the component breaks in an unstable manner due to increasingly large crack growth (Zehnder 2012, p. 72).

3.5.4 Paris-Erdogan, and its Application to Fatigue Assessment

The middle region in Figure 5, region two represents the growth of a crack. As stated in the previous subchapter, the middle region is known as the Paris' region which can be represented by one of the most widely known crack propagation laws, and it was arrived at through experimentation by P. Paris with help from F. Erdogan. (Paris 1962.). The Paris law in its original form is presented as:

$$\frac{da}{d\mathrm{N}} = \frac{(\Delta K)^4}{\mathrm{M}} \tag{22}$$

Where M is a material parameter that depends on frequency, mean load, environmental conditions and other related variables, a is the size of the crack and N refers to the number

of cycles. According to Paris (1962), the aforementioned relationship appeared to fit fairly well to experimental test data using a slope parameter of ¼.

More modernly, the material parameter M was instead changed to a variable that depends on material properties and the slope parameter of ¼ was changed to a distinct slope parameter that also depends on the material used. Commonly, *m*, and the slope parameter has a value somewhere between two and four. (Dowling 2013, p. 566.) When discussing Paris' law today, it may be written as:

$$\frac{da}{d\mathrm{N}} = \mathrm{C}(\Delta K)^{\mathrm{m}} \tag{23}$$

Where C and m are parameters related to the material properties.

As Paris' law contains a variable for the number of cycles, the expression can be manipulated to obtain the fatigue life of a given component assuming certain conditions are fulfilled. The approach produces a conservative fatigue life estimate near the first region due to the fact that Paris' law is approximately a straight line on a log-log scale whereas the first region is very non-linear. As for region three, the Paris' leads to an unsafe approximation due an almost asymptotic crack growth rate. (Pook 2007, pp. 122-123.) To obtain the fatigue life using Paris' law, the first step is to rearrange Equation 23 and expand the term for SIF range as described by:

$$\frac{d\mathrm{N}}{da} = \frac{1}{\mathrm{C}(\Delta K)^{\mathrm{m}}} = \frac{1}{\mathrm{C}\left(\Delta\sigma\,\mathrm{Y}\sqrt{\pi a}\right)^{\mathrm{m}}} \tag{24}$$

Where Y is a geometry dependent factor for correcting the value of SIF. Equation 24 can be solved as a separable first order differential equation by multiplying both sides by *da* and then subsequently integrating the rearranged equation. The result of the integration is shown by:

$$N = \int_{a_i}^{a_f} \frac{da}{C\left(\Delta\sigma\, Y\sqrt{\pi a}\right)^m} = \frac{a_f^{\left(1-\frac{m}{2}\right)} - a_i^{\left(1-\frac{m}{2}\right)}}{C\left(\Delta\sigma\, Y\sqrt{\pi}\right)^m \left(1-\frac{m}{2}\right)} \quad (25)$$

Where a_i is the size of the initial crack and a_f is the size of the crack at the end to the fatigue life. According to Dowling (2013, p. 594), typically the value for final crack size needs to be ascertained before proceeding to determine the number of cycles to failure. Since the value for SIF also depends on the size of the crack, the process through which the final crack size needs to be obtained through is an iterative process where the size of the crack at the end of the fatigue life is where the SIF is equivalent to the fracture toughness of the material.

3.6 Fatigue of Notched Components

The link between the initiation of a fatigue crack and a discontinuity in the parent material is the amplified stress caused due to the change in the local geometry. These localised discontinuities are otherwise known as notches that can be the results of a manufacturing defect or simply a feature of the component itself where one section is smaller than the next. In such discontinuities, when the applied force travels through a narrower path, the stress increases locally at the notch root. (Schijve 2009, pp. 171-172.)

The behaviour of notched components under cyclic loading conditions depends also on the approach to fatigue assessment. Therefore, this chapter shall be divided into three parts, the first of which concerns with the stress-life approach and the second section will focus on the strain-life approach. Lastly, the chapter concludes with how the effect of notches is considered in fracture mechanics.

3.6.1 Notches in S-N Approach

In the S-N approach, the influence of notches can be described using a relationship between the maximum stress at the root of the notch due to the applied load and the corresponding stress throughout the cross-section of the component. This relationship is known as the elastic stress concentration factor. (Nicholas 2006, pp. 213-214.) The elastic stress concentration factor is defined as:

$$K_t = \frac{\sigma_{peak}}{\sigma_{net}} \tag{26}$$

Where σ_{peak} is the maximum stress experienced by the material at the root of the notch and σ_{net} is the stress acting on the net cross-section far away from discontinuities. The elastic stress concentration factor K_t depends solely on the geometry of the notch. There exist ready-made curves for use in common engineering applications. However, due to its simplicity, the method can produce erroneous results if applied to more complex situations. (Nicholas 2006, pp. 214-215.) Because the material response at the root of the notch depends on more than just the geometry of the specimen. More accurate models for estimating the notch effect have been developed One such improved model is the fatigue notch factor. Fatigue notch factor takes the form:

$$K_f = \frac{\sigma_{smooth}}{\sigma_{notch}} \tag{27}$$

Where σ_{smooth} is the fatigue limit stress in a smooth component or a component without notches and σ_{notch} is fatigue limit stress in a notched component. While the expressions 26 and 27 appear similar, Equation 27 involves more than just the maximum stress in the notch, rather, it is a combination of the stress or strain state over the material volume and geometrical factors such as the radius of the notch root. Experimental data has also been used to verify that that the use of K_f produces a more accurate estimate of the effect of notches. (Nicholas 2006, pp. 216-217.)

The value for K_f is typically less than or equal to the value of K_t depending on the strength of the material as well as the size of notch. For example, in materials with a low tensile strength in combination with a sharp notch, the difference between the two quantities can be significant in comparison to a material with a high tensile strength and a sharp notch. In essence, this means that some materials are affected more by notches than others. (Schijve 2009, pp. 174-176.) This is referred to as notch sensitivity, and it can be formulated as:

$$q = \frac{K_f - 1}{K_t - 1} = \frac{1}{1 + \frac{a^*}{\rho}} \tag{28}$$

Where a^* is material dependent constant and ρ is the radius of the notch root. Peterson observed that for zero mean stress, Equation 28 was a reasonably good fit for estimating specimens notch sensitivity. According Schijve (2009, pp. 177-181), there exist also alternative experimental methods for obtaining the notch sensitivity, namely by Neuber and Siebel.

The presence of notches clearly has been shown to have a negative influence on the fatigue life of a machine component. The degree to which notches reduce fatigue life depends on the material as well as the notch geometry, surface finish and mean stress level. For example, tests on SAE 4130 steel have shown that the fatigue limit for notched specimens depending on the geometry could be as low as one third of the fatigue limit of a smooth specimen made from identical material. (Schijve 2009, pp. 202-206.)

A 2025 research paper on the influence of pores on fatigue life of wire arc additively manufactured aluminium (Al) alloys, by Safyari and Moshtaghi investigated how pores, as a result of the manufacturing process act as notches that cause localized increases in stress. The results indicated that fatigue performance was mainly governed by the size of the pore, with larger pores resulting in the largest drop in fatigue life. Conversely, smaller and uniformly distributed pores resulted in smaller stress concentrations and consequently, increased fatigue life. Ultra-fine distribution of pores could even result in favourable conditions in terms of fatigue life, regardless of the number of pores.

3.6.2 Notches in ε-N Approach

The treatment of notches in the strain-based approach depends on the degree of yielding in the notch root which is described using one of the three distinct phases of material response. The first of which is a state where no yielding occurs. In the first phase, the applied load does not exceed the yield strength of the material. The second phase consist of localized yielding, and lastly, fully plastic yielding. The state of elastic yielding can be represented by a linear relationship where the local material response in terms of stress correlates linearly

with the stress concentration factor. The elastic strain corresponding to the stress is therefore a linear relationship that depends on the slope of the line, or the Young's modulus. (Dowling 2013, p. 712.) The relationship can be written as:

$$\varepsilon = \frac{K_t \sigma_{nom}}{E} \tag{29}$$

Where σ_{nom} is the applied nominal stress. The applied stress can be caused by any type of load. For cases where the applied load results in either localized or fully plastic yielding, the approach changes slightly to account for the permanent changes in the material. (Dowling 2013, pp. 713-714.)

One such approach for estimating the material response at the notch root is the Neuber's rule which equates the mean stress- and strain concentration factors to the value of K_t^2. The statement holds true for plastic deformation because the ratio of notch strain to nominal strain stays above the value of K_t whereas in the case of notch stress, the opposite occurs, making the equivalent mean equal to K_t. The aforementioned statement can be simplified into a single expression as shown below:

$$\sigma\varepsilon = \frac{(K_t \sigma_{nom})^2}{E} \tag{30}$$

Depending then on the utilized material model, the strain at the root of the notch can be obtained using different approaches that can be defined as follows:

$$\varepsilon = \frac{(K_t \sigma_{nom})^2}{\sigma_y E} \tag{31a}$$

$$\varepsilon = \left[\frac{(K_t \sigma_{nom})^2}{EH'} \right]^{\frac{1}{(n'+1)}} \tag{31b}$$

Where σ_y is the yield strength of the material, H' is the cyclic hardening coefficient and n' is the cyclic hardening exponent. Equation 31a is applicable for an elastic-fully plastic material model meaning that once the stress at the root of the notch has reached the yield strength of the material, no further increase in stress can occur, only the value of strain increases. Whereas Equation 31b uses the power-hardening model, where the effect of strain hardening is included in the material response. The model shown by Equation 31b allows for the estimation of strain post-yielding at the root of the notch. (Dowling 2013, pp. 715-716.)

The process through which the fatigue life is determined using a strain-based approach is more involved than for stress-based methods. According to Dowling (2013, pp. 771-774), it begins with determining and calculating the case specific initial information such as load type and material constants. Then the material response at the notch can be obtained by using the methods introduced in this subchapter. Once the material response is determined, a plot of the material response is drawn to obtain the stresses and strains at any given point of the load cycle. Lastly, by utilizing the information determined from the previous steps, the fatigue life of the component can be calculated using one of the strain-based assessment methods such as Morrow, SWT or Walker.

3.6.3 Notches in Fracture Mechanics

Notches in fracture mechanics concern primarily with the growth of fatigue cracks that begin from notches. According to Ellyin (1996, pp. 400-403), the growth of cracks that begin from a notch are divided into sharp and blunt cracks where the former can have a tendency to become non-propagating due to insufficiently large bulk stress. For sharp notches, as the crack grows beyond a certain point, it is possible for the rate of crack growth to slow down. As the rate of growth slows down, the growth of a crack does too and even stop. In case of a blunt crack, if the crack propagates, it propagates to failure because to initiate a crack in a blunt notch, the stress must be large enough to initiate at the notch, once a crack is formed, the bulk stress remains large enough to maintain a high crack growth rate until the specimen breaks.

The process of crack growth follows principally the laws presented in the previous chapter on fracture mechanics and need not be reiterated here, only a distinction shall be made with regard to where they apply. The distinction concerns with LEFMs' application to longer

cracks. The previously presented laws can only be applied to a situation where the bulk stress is so large as to be able to grow a crack until the component fails. As short cracks can become non-propagating, they must be treated separately. (Ellyin 1996, p. 404.)

Short cracks can bring about limitations that prevent the use of LEFM outright in fatigue assessment. One such limitation is the size of the plastic zone at the notch root. Dowling (1979) argued that even a moderate degree of yielding in a sharp notch can result in a plastic zone that dominates the entire region of the small crack leading to a situation where the precondition for LEFM, more specifically the small-scale yielding requirement is not fulfilled. If the condition for small-scale yielding is not fulfilled, elastic-plastic fracture mechanics would have to be employed instead.

For small cracks that are applicable for LEFM, methods based on the behaviour of microstructure are preferred where the objective is to model the process by which small cracks grow. Ellyin (1996, pp. 437-438) introduces a model based on effective stress intensity factor range to imply that there exists a link between small crack growth and SIF range. Two models by two research teams were developed. First by Tanaka. K and Nakai. Y in 1983 who observed that the difference between short and long crack growth rate could be bridged better if they were included as a function of the effective SIF range. A second model is by Newman and his team who came up with a crack closure approach that could estimate when a condition of steady state crack closure is reached after the crack grows to a certain size. Newman et al. were able to conclude that the effective SIF range did not appear to correlate long and short crack growth which contradicts what Tanak and Nakai found, but the differences could be explained by the values for the crack opening stress. In closing, the effective SIF range approach does not completely account for the growth of small crack because is deals with plasticity induced crack closure completely and not test data which is why LEFM can erroneously predict the effect of notches in fracture mechanics. The effective SIF range method can still be utilized although the veracity of the results should be contrasted with experimental data.

3.7 Variable-Amplitude Fatigue

Heretofore, discussion related to fatigue has focused primarily on constant amplitude loading. According to Frost et al. (1999, p. 307), fatigue tests are typically carried out with

a constant amplitude cyclic load. However, during operation, machinery components can and often are subjected to cyclic loads with a varying stress amplitude. Further, the loads occurring in real-life may also be random, which creates a situation where the degrees of damage they cause to the component varies over time and makes the assessment of fatigue life more complicated. According to Stephens et al. (2001, p. 274), damage in the context of fatigue refers to the portion of the total life that a component can withstand before failure occurs. When the component finally breaks due to repeated loading, the amount of damage that has accumulated is 100 %. As the underlying principles of fatigue as a phenomenon remain intact, this chapter shall focus only on relevant theories to account for the effect of variable amplitude loading on fatigue life and on how irregular loading histories are treated.

3.7.1 Treatment of Irregular Load History

Two of the most commonly used methods for dealing with irregular load histories are the rainflow method and the reservoir method. both of these methods produce the same result in the end. These two methods are the most popular due to the fact that they tend to predict the most conservative damage estimates and because they are relatively simple to use. This is because both methods treat each load cycle independently, and in the presence of randomly applied cycles with large stress amplitudes and mean stresses, thus making up for a larger part of the total damage. (Stephens et al. 2001, p. 281.) An example of an irregular load history is presented in Figure 6.

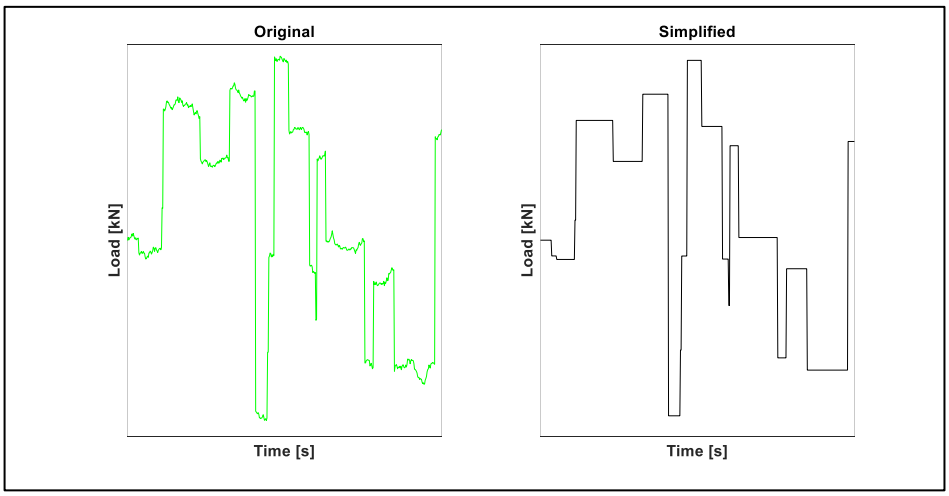

Figure 6. Irregular load history

Figure 6 shows two plots, on the left side represents an example of a real-life load and on the right, a simplified version of it. The simplified version is often necessarily created to remove additional noise that would just complicate the analysis, especially if the fatigue analysis is conducted analytically without the aid of numerical tools.

Both rainflow-counting and reservoir methods are analogous to practical, everyday concepts and therefore easy to understand and apply. In the rainflow-counting approach, a load history is conceptually turned on its side such that the abscissa and ordinate are rotated by 90 degrees clockwise. While a rotated load history such the one shown by Figure 6 doesn't exactly resemble the roof of a pagoda, if rain begins to flow from the largest peak or the lowest valley towards the bottom until the next load reversal or a point that stops the flow path. The path of the flowing water essentially closes a stress range as a single cycle. This process is repeated until every load reversal has been accounted. (Stephens et al. 2001, pp. 282-286.)

The reservoir method is arguably even easier to understand. According to Gurney (2006, pp. 106-107), the load history is arranged so that the observation range is between the largest stress or load peaks representing a kind of a container. This imaginary container is then filled with water by drawing a straight line between the largest peaks, and then through process of elimination, each cycle as represented by a stress range is counted by emptying the corresponding stress range of water. Each range is subsequently drained until the whole container is empty of the imaginary water. The main objective of both rainflow counting or the reservoir method is to determine the number of different load cycles and the corresponding stress range, stress amplitude and mean stress. After the number of different cycles has been determined, fatigue assessment moves onto the next phase, the estimation of damage.

3.7.2 Palmgren-Miner Damage Theory

One of the most widely known damage theories is by Palmgren and Miner. Originally it was Palmgren who first published a paper explaining the concept. Later, Miner independently came up with the same idea, but it was through Miners' publication that the method became popular and remains so even today. The approach states that the ratio of applied load cycles to the total number of cycles the component is able to withstand is equal to one. (Gurney 2006, pp. 111-112.) The Palmgren-Miner damage theory can be defined as:

$$\frac{n_1}{N_1}+\frac{n_2}{N_2}+\ldots+\frac{n_i}{N_i}=\sum\frac{n}{N}=1 \tag{32}$$

Where n is the number of applied load cycles and N is the number of total cycles. However, while the Palmgren-Miner approach is simple, it comes with a lot of underlying assumptions that have proven to be untrue. According to Andersson (2021, pp. 118-119), the method can both overestimate and underestimate the degree of damage because it does not account for crack growth retardation and acceleration, or the load sequence effect. For example, if the initial loading is a deliberate tensile overload, then as a result of the overload, a compressive residual stress state remains in the material after unloading, resulting in a situation where the rate of crack growth slows down for a while. Alternatively, if the initial overload was on the compressive side, the result would be a tensile residual stress state which consequently accelerates crack growth for the subsequent cycles. Data from experimental tests has shown that for different stress ranges and amplitudes, the total damage is not necessarily one or 100 % but somewhere between 0.2 and 5.

This is not to denigrate the approach, rather with a thoughtful attitude and while minding the potential pitfalls, the Palmgren-Miner is an excellent tool applicable to the initial stages of fatigue analysis process. Palmgren-Miner can be especially useful if used in combination with experimental fatigue testing as part of component design. (Frost et al. 1999, p. 330).

3.7.3 Alternative Damage Theories

Pitfalls with the linear damage theory by Palmgren and Miner has given rise to alternative models in an attempt to come up with an approach that agrees with experimental data more accurately.

Based on an extensive survey of existing damage theories by Fatemi & Yang (1998), there are multiple alternatives based off different principles. These include nonlinear models such as the Marco-Starkey approach which attempts to include the effect load sequence by utilizing a power relationship with a nonlinear exponent. By utilizing a nonlinear exponent, the Marco-Starkey approach adjusts the degree of damage with the corresponding level of stress to account for the effect load sequence.

Methods based off crack growth also exists. For example, the Wheeler method which relates the rate of crack growth to the relationship between the crack tip plastic zone and the compressive residual stress in the event of an overload by multiplying Paris' law with an empirical retardation factor. The empirical retardation factor then relates the size of the crack tip plastic zone to the magnitude of the applied load resulting in a factor that either slows down or speeds up the rate of crack growth, indicating the presence or absence of overload. (Fatemi & Yang 1998.)

There are also approaches based on the S-N curve like the one by Subramanyan, which suggests that damage accumulation can be thought of as the ratio of the slope of an isodamage line corresponding to specific amount of damage with respect to the slope of the original S-N curve. As the isodamage lines run parallel to the S-N curve, it follows that the fatigue limit is constant except for the point corresponding to the fatigue limit due to a singularity caused by two reasons, namely the fact that each isoline crosses this point, and because of the non-linear nature of the S-N curve near the fatigue limit. (Fatemi & Yang 1998.)

Despite multiple different methods that take advantage of non-linearity, fracture mechanics, continuum mechanics or strain energy density, the approach towards variable amplitude loading remains complicated. According to Stephens et al. (2001, p. 277), Palmgren-Miner remains still the most commonly used method even though it has some problems. However, regardless of its problems, it outshines the alternative methods by its simplicity and ease of use.

3.8 Multiaxial Fatigue

In the same way that real-life load histories rarely consist of constant-amplitude loading, machine components in real-life are also rarely subjected to completely uniaxial stress state. For common machinery components in operation, the stresses as a result of the applied forces are more often than not multiaxial. Multiaxial stress state refers to a condition, where stresses act in different directions at the same time instead of along one of the three principal axes x, y or z. A fundamental difference between uniaxial and multiaxial stress state can be explained by using the proportionality of loads with respect to other loads acting at same time. In a uniaxial plane stress state with two simultaneous stress components acting at the

same time, it can be said to be proportional if the stress components act synchronously. Conversely, in the case of a non-proportional load, there exists a phase difference between the acting stress components. (Milella 2024, pp. 593-595.)

The objective of this chapter is to examine commonly used stress, critical plane and fracture mechanics-based criteria for multiaxial fatigue and fatigue life assessment.

3.8.1 Stress-based Approach

Arguably, one of the most well-known stress-based criteria for evaluating multiaxial stress state in the field of engineering is the octahedral shear stress theory, otherwise known as the Von Mises criterion and it can be presented by:

$$\sigma_{eq}=\frac{1}{\sqrt{2}}\sqrt{(\sigma_{a1}-\sigma_{a2})^2+(\sigma_{a2}-\sigma_{a3})^2+(\sigma_{a3}-\sigma_{a1})^2} \quad (33)$$

Where σ_{a1} is the principal alternating nominal stress, where the lowest subscript indicates the largest stress magnitude. According to Stephens et al. (2001, pp. 322-325), the Von Mises stress criterion represents an equivalent stress that is made up of the individual stress components, such as axial, bending, and shear stress. In the field of engineering, the Von Mises criterion is commonly used for evaluating ductile materials. The reason for its popularity is due to its simplicity. However, Von Mises equivalent stress does not account for hydrostatic stress, meaning that it neglects the effects of mean stress on fatigue life. Equivalent stress methods are also relatively inaccurate when used with disproportional loads and should therefore be applied for cases where the stresses act along the principal axes and that the axes do not change direction when the component is loaded. In a biaxial stress state, Von Mises can be plotted as an ellipse, like the one shown in Figure 7.

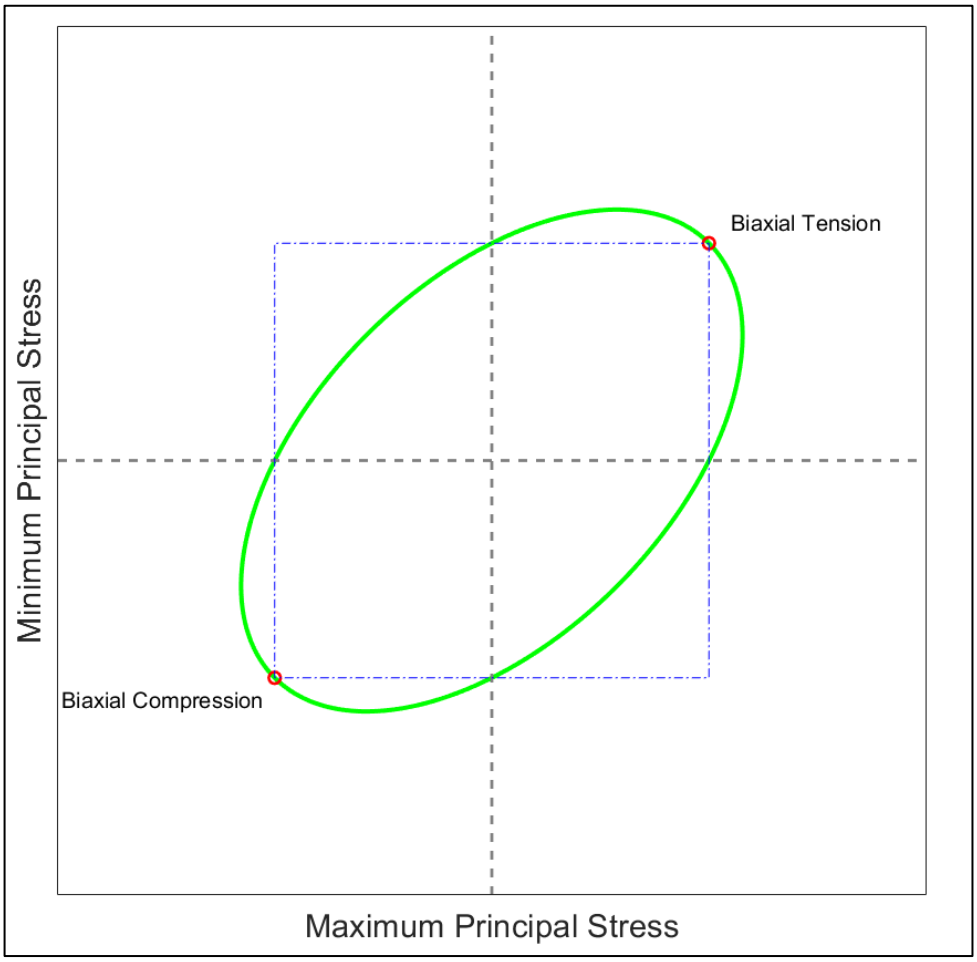

Figure 7. Biaxial stress envelopes, Von Mises vs. Max. Principal

Figure 7 shows an ellipse that represents the limit for yielding under biaxial stress state. If the equivalent stress acting on a machinery component exceeds the boundaries of the ellipse, the component undergoes permanent deformation, and the Von Mises theory no longer applies. The blue rectangle in the same figure represents the maximum principal stress theory which is used for comparison to indicate the difference between the two theories. The maximum principal stress theory does not account for the effects of shear stress nor the orientation of stress planes and as a result, does not agree well with ductile materials but instead works rather well for brittle materials. The different methods utilizing equivalent stresses are often used because they are convenient, but they can result in erroneous results if used for estimating non-proportional loading conditions. For non-proportional loads, methods based on the critical plane or energy should be considered. (Stephens et al. 2001, pp. 324-329.)

3.8.2 Critical Plane Approach

Based on observations from experimental fatigue tests, the formation of cracks begins from distinct planes. More specifically, cracks begin on the plane of maximum shear or tensile stress where persistent slip bands form. Methods based on the critical plane operate on the assumption that any stress or strain acting normal to the most stressed plane opens the micro crack thus releasing the mechanical interlocking effect making it easier for the crack to grow. Once a crack forms on one of these critical planes it will propagate until the component fails. To determine which plane is the critical plane, the maximum resolved shear stress is replaced with the maximum shear stress. The critical plane will then be where the highest stresses occur. Consequently, this will be the plane on which fatigue cracks grow until failure. A commonly applied critical plane approach is a modification to the Brown-Miller approach by Fatemi and Socie. (Milella 2024, p. 613.) The correction by Fatemi and Socie is presented as:

$$\gamma_{max}\left(1+\kappa_{FS}\frac{\sigma_{n,max}}{\sigma_y}\right)=\text{Constant} \tag{34}$$

Where γ_{max} is the maximum shear strain, κ_{FS} is a material constant, and $\sigma_{n,max}$ is the maximum normal stress. The reason why the maximum normal stress is divided by the yield strength of the material is so that the result is unitless, as strain typically is. According to Milella (2024, pp. 617-618), the Fatemi-Socie approach is not a standalone model but instead an improvement on the Brown-Miller approach. The difference being that in the model by Fatemi and Socie, variables related to the range of shear strain which were replaced by the maximum stress acting perpendicular to the plane of maximum shear strain, which resolved the issue caused by micro-crack having the same value for the maximum shear strain range and the range of shear strain.

The Fatemi-Socie can be extended to obtain fatigue life as well by rewriting the right-hand side of the equation using uniaxial shear strain-life properties. With this approach, the method has been applied for a wide range of applications where shear fatigue is relevant. Results from experimental testing have also revealed that the Fatemi-Socie method works

very well for both proportional and non-proportional loading conditions for many different materials, even high strength steel alloys. (Stephens et al. 2001, pp. 331-332.)

3.8.3 Multiaxial Fracture Mechanics

Multiaxial fatigue from the viewpoint of fracture mechanics takes the form of crack growth occurring with multiple opening modes at the same time. The combination of opening modes depends on the applied loading, its direction and the component itself. For example, a plate with an edge crack under three-point bending will experience crack growth according to modes one and two. However, for plates in general, the initial mixed mode crack growth will eventually lead to crack growth according to crack opening mode one. (Stephens et al. 2001, p. 337.)

According to Stephens et al. (2001, pp. 337-338), multiple different methods exist for dealing with mixed mode crack growth. For cases, where the size of the crack tip plastic zone is within an acceptable range for LEFM, an equivalent SIF range approach works. But if the plastic zone is sufficiently large, alternative methods should be considered such as approaches based on strain energy density or the J-integral. The equivalent SIF range method can be expressed as:

$$\Delta K_{eq} = \left(\Delta K_I^4 + 8\Delta K_{II}^4 + \frac{8\Delta K_{III}^4}{1-\nu} \right)^{0.25} \tag{35}$$

Where ν is the Poisson's ratio. Equation 35 represents one of the most commonly applied equivalent SIF range approaches. It was originally proposed by K. Tanaka in 1974. Tanakas' method operates based on crack tip displacement which takes the form of an equivalent stress intensity factor range where all three modes are combined together. The expression also reveals that modes two and three are weighted meaning that the opening modes related to shear appear to be more dominant. Once the equivalent SIF range has been determined, the fatigue assessment can be done using Paris' crack growth law. (Stephens et al. 2001, pp. 337-338.)

3.9 Experimental Setup

This subchapter on experimental testing describes the procedures undertaken to assess the microstructure and fatigue performance of the Hadfield steel specimens. These procedures include specimen preparation, hardness testing, metallographic analysis, and fatigue testing.

3.9.1 Hardness testing, Grain size analysis, Optical microscopy and SEM

A total of four test specimens were prepared, two for each sample. One of the samples was allocated for hardness testing and optical microscopy, while the other was solely for SEM. Separate specimens for both were created because hardness testing creates indents on the surface of the specimen causing potential distortion due to the locally deformed surface.

The test specimens were cut from round bar stock of cast Hadfield steel into thin discs. The Hadfield steel discs were subsequently embedded into conducting epoxy to simplify sample preparation. Embedding the specimens in conductive epoxy also removes the need to use conductive tape with SEM. The surface of each of the four samples were then ground, polished to a mirror-like and etched. A 4% Nital solution was used to etch the specimens. Lastly, the specimens were rinsed and dried.

Hardness testing

The hardness tests were performed with a Struers DuraScan micro hardness tester utilizing the Vickers method as specified according to EN-ISO 6507-1:2023. The tests were carried out using a 3 kgf load. Microhardness of the Hadfield steel specimens were measured at 25 test points as shown in Figure 8.

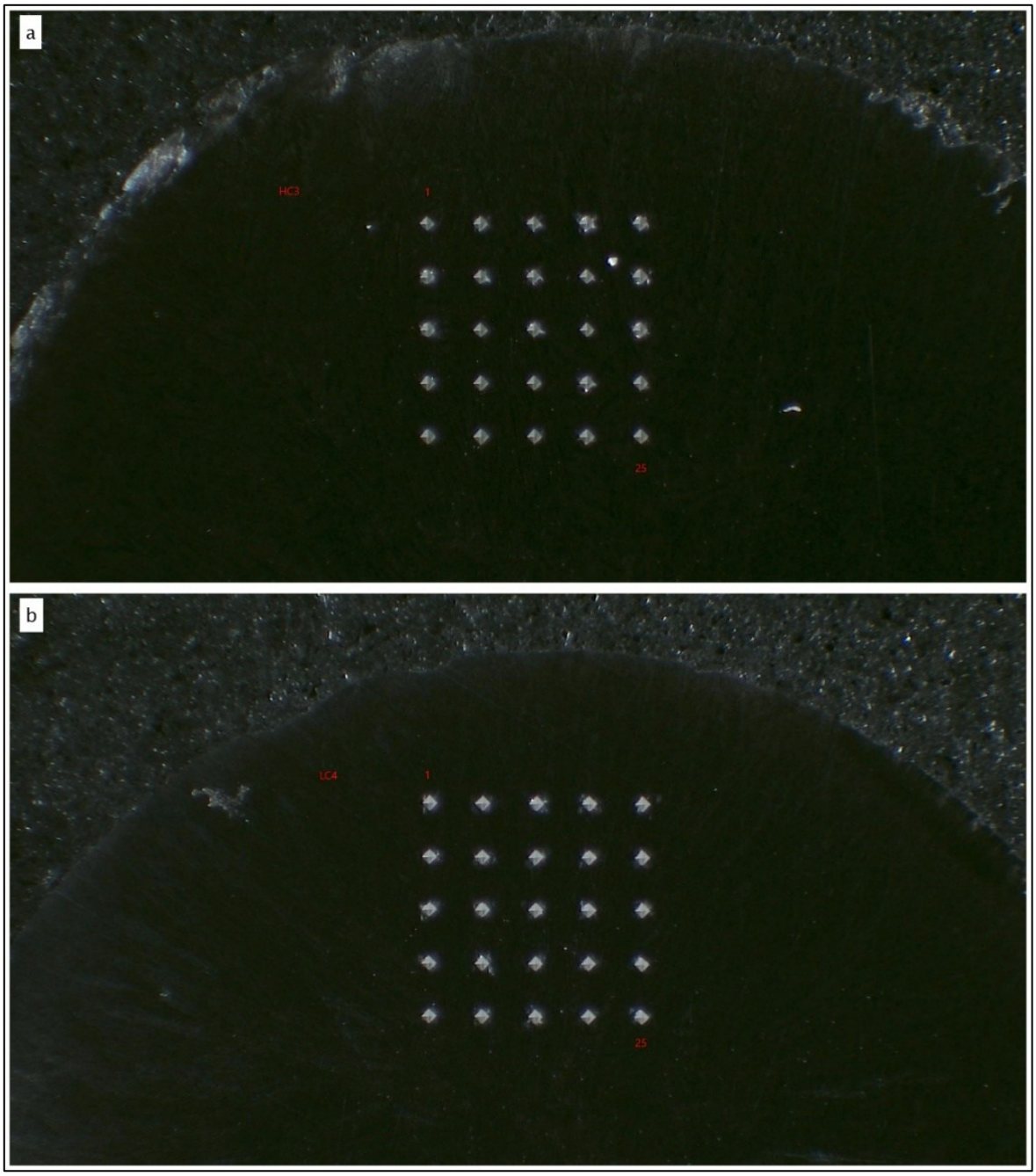

Figure 8. Macroscope image of the hardness test points a) Specimen 1, HC, b) Specimen 2, LC

The test points in both specimens shown by Figure 8 are placed in the upper quadrant of the Hadfield steel disc and they are located 0.5 mm apart from each other in rows of five. The first point is located close to the surface of the specimen whereas the 25th point is closer towards the centre.

Metallography

The Hadfield steel samples were examined under both an optical microscope and SEM. The optical microscopy was done using Meiji IM7200 brightfield metallurgical microscope. The photomicrographs were provided with a 100 µm reference scale which was used for subsequent measurements. The grain size measurements were carried out using ToupView.

SEM related work was carried out using Hitachi SU3500 with a secondary electron (SE) and backscatter electron (BSE) detectors. The accelerating voltage was set to 15 kV. Images were captured with a magnification range of x42 – x10k.

Additionally, energy-dispersive X-ray spectroscopy (EDS) was used to investigate the chemical composition of selected features in both HC and LC specimens, using both general mapping to get an overview of the distribution of elements, as well as point analysis to identify specific features.

Grain size analysis

The grain size of the Hadfield steel specimens was determined according to EN ISO 643:2024 using the linear intercept method. In the linear intercept method, individual or groups of straight lines of known length are drawn at arbitrary locations onto the photomicrograph. Then the number of grain boundary intersections are counted along each line (SFS-EN 643:2024, p.16).

Once the number of intersections has been counted, the mean number of intersections for every millimetre is determined using the following expression:

$$\overline{P}_L = \frac{\overline{P}}{L_T} \tag{36}$$

where, $\overline{P}$ is the mean value of the number of intersections and L_T is the true length of the test line divided by the magnification, in millimetres. The final step in determining the grain size is to compute the mean lineal intercept range which is obtained as follows:

$$l = \frac{1}{\overline{P}_L} \tag{37}$$

The nominal value for the mean lineal interception length can then be compared to the limit values corresponding to the grain size indices shown in SFS-EN 643:2024 (Table 3). The higher the value for G, the smaller the grain size.

To ensure the reliability of the measurements, a maximum relative error of 8.5% was adhered to as per SFS-EN 643:2024 recommendation.

3.9.2 Fatigue Testing

Fatigue testing was conducted using an MTS servohydraulic testing machine. A total of 17 specimens were tested across two variants, nine of which were for the HC variant and eight for the LC.

The tests were conducted under load-controlled conditions with an applied cyclic load at a specific load amplitude. The applied loading parameters are presented in Table 2, which lists the stress amplitude and R.

Table 2. Fatigue testing parameters for HC and LC specimens

Specimen	σ_a [MPa]	R
HC_1	680	0.1
HC_2	535	0.1
HC_3	590	0.1
HC_4	685	0.1
HC_5	425	0.1
HC_6	345	0.1
HC_7	390	0.1
HC_8	335	0.1
HC_9	315	0.1
LC_1	570	0.1
LC_2	590	0.1
LC_3	445	0.1
LC_4	505	0.1
LC_5	410	0.1
LC_6	305	0.1
LC_7	310	0.1
LC_8	305	0.1

The fatigue tests were carried out under constant frequency of 15 Hz in ambient temperature. Failure of the tests specimens was defined as the specimen fracturing completely.

4 Results and Discussion

The results presented in this chapter are comprised of assessing the mechanical performance and microstructural properties of Hadfield steel specimens. The results include hardness testing, metallographic analyses, as well as fatigue testing. Hardness testing was used to evaluate the microhardness distribution of the specimen's cross-sections. Metallographic investigation was conducted using an optical microscope, as well as SEM and EDS, all of which provided valuable information about the microstructure and its relation to fatigue performance. Fatigue testing was accomplished using MTS servohydraulic testing machine the results of which was used to obtain the fatigue strength of both test specimens in low and high cycle regimes. This chapter contains both the obtained results as well as their analysis and discussion, beginning with hardness testing, followed by metallographic investigation, and finally fatigue testing, where each subchapter builds on the previous, providing a comprehensive understanding of the material.

4.1 Hardness tests

The results of the hardness tests provide insight into the delivery condition of the test specimens, namely into the microhardness across the cross-section of the cast Hadfield steel specimens. The measured hardness values of the high- and low-carbon Hadfield steel specimens are presented in Table 3.

Table 3. Hardness values for test specimens HC and LC.

Test Point	Specimen 1, HC		Specimen 2, LC	
	Diagonal (µm)	Hardness [HV]	Diagonal [µm]	Hardness [HV]
1	136,473	299	141,692	277
2	138,556	290	142,189	275
3	140,114	283	142,422	274
4	147,917	254	144,03	268
5	143,312	271	145,064	264
6	139,329	287	140,118	283
7	137,51	294	140,892	280
8	138,325	291	140,657	281
9	140,365	282	142,45	274
10	149,481	249	141,436	278
11	139,354	286	139,066	288
12	138,031	292	140,379	282
13	144,421	267	141,671	277
14	136,208	300	141,171	279
15	149,604	249	142,223	275
16	145,838	262	140,635	281
17	146,887	258	138,185	291
18	143,235	271	139,329	287
19	147,68	255	142,975	272
20	139,329	287	139,599	285
21	146,633	259	141,686	277
22	150,782	245	139,355	286
23	145,578	262	139,844	284
24	145,858	261	144,03	268
25	142,715	273	139,092	288

The hardness of the HC sample ranged from a maximum value of 300 HV to a minimum of 245 HV, with an average of 273 HV. In comparison, the maximum value for hardness in the LC sample was 291 HV and the lowest value was 264 HV resulting in an average hardness of 279 HV. To better illustrate the change in hardness throughout the specimens, the values presented in Table 3 are illustrated. The hardness distribution in the HC specimen is shown by the following figure, Figure 9.

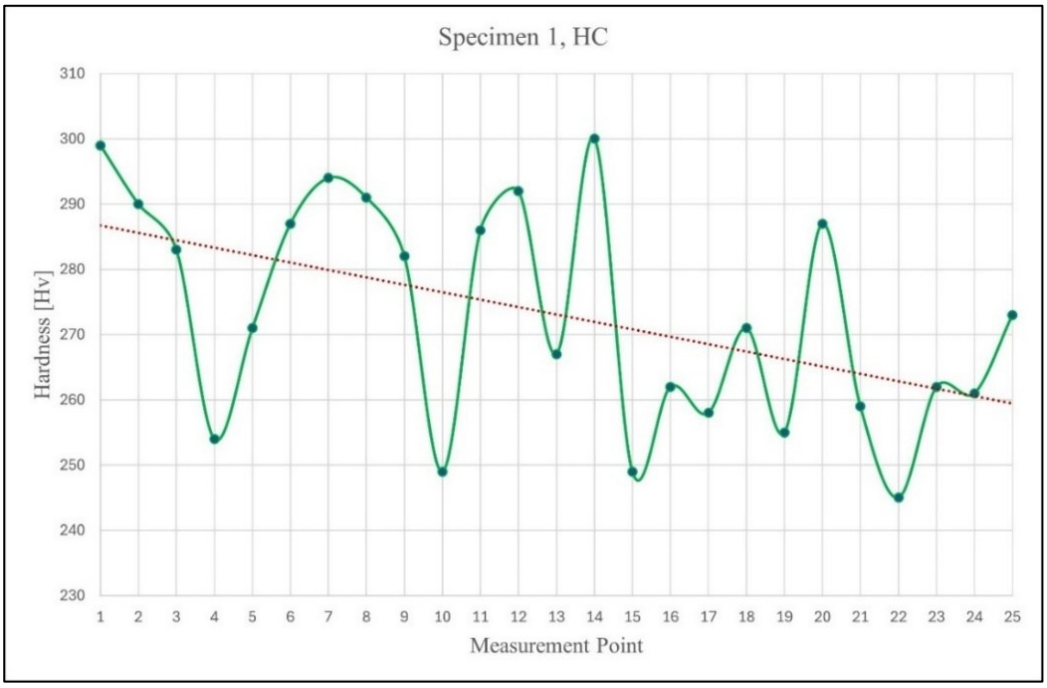

Figure 9. Hardness distribution, HC

Based on the hardness values from Table 2 and the red trend line in Figure 9, the hardness of the HC specimen decreases gradually towards the centre of the cross-section. In comparison, the low-carbon specimen reveals the opposite behaviour where the hardness increases towards the core. The hardness distribution in the LC specimen is shown by Figure 10.

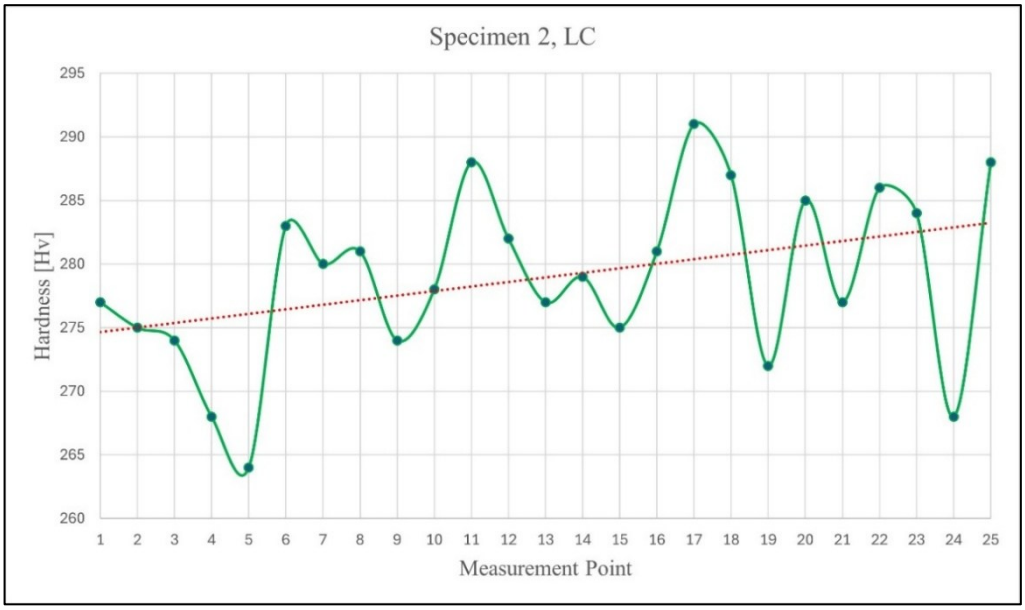

Figure 10. Hardness distribution, LC

Based on the hardness values shown by Table 3 in combination with the trend line in Figure 10, it can be observed that the hardness increases slightly towards to core of the specimen. The trends in hardness can be explained better by comparing them to values of hardness reported in the literature.

The measured hardness values for both specimens are within the range of typical austenitic manganese steel grades in as-cast condition. According to Subramanyam et al. 1990, pp. 1970-1977; Miekk-oja et al. 1986, p. 432, the value of hardness for most common grades is around 200 HV, but depending on the specific chemical composition, the hardness values can vary between 200-300 HV.

Although the average hardness of the high- and low-carbon specimens were reasonably close to each other, the distribution of hardness across the cross-section revealed opposite trends. In the HC variant, the higher hardness near the surface and lower values toward the core are consistent with expected results. The increased surface hardness may be a result of local deformation during specimen preparation. The nature of Hadfield steel is such that during cutting, a thin hardened layer can develop in the vicinity of the start of the cut. However, since both specimens were prepared identically, a similar increase in hardness near the surface of the low-carbon sample should also be observed. A more likely explanation for the opposite trend in the low-carbon specimen is related to carbide formation. Subramanyam et al. (1990, pp. 1970-1977) explain that in higher-carbon Hadfield steels, carbides form along grain boundaries and interdendritic regions and even within the austenite matrix itself. With an increased carbon content, the temperature required to dissolve carbides also increases resulting in an alloy comprised of austenite and carbide which is harder than pure austenite.

With increased C content, the amount of carbide formation also increases. An increase in the volume fraction of carbides such as alloyed cementite within the austenite matrix and grain boundaries can results in increased hardness. The microhardness of alloyed cementite can vary between 1030-1270 HV0.02. While increasing C also increases the amount of carbides, it also increases the wear resistance, but does so at the expense of toughness, and by making the alloy more brittle (Tecza & Garbacz-Klempka 2016).

The contrasting values for hardness between the two different specimens warrant further investigation of their microstructure using both optical microscope and SEM to better understand the role of carbon in Hadfield steel. Since the focus of this thesis is fatigue

assessment, it is important also to observe how differences in hardness and chemical composition, namely carbon content influences fatigue performance.

4.2 Metallography

Complementary to the microhardness results, the Hadfield steel specimens were also investigated using an optical microscope as well as SEM. The analyses focused on observing the grain structure as well as the presence of secondary phases and inclusions which may influence the fatigue performance. The subsequent figures present the microstructure of both specimens beginning with optical microscopy. The microstructure of the HC Hadfield steel specimen is presented in Figure 11.

Figure 11. HC specimen micrograph.

The micrograph of the HC variant reveals clear and distinct grain boundaries. In addition, multiple small and a few relatively large darker features are scattered throughout the material. The low-carbon sample is presented in Figure 12.

Figure 12. LC specimen micrograph.

Similarly to the HC variant, the LC sample displays identical dark features both small and large. The difference between the two specimens based on the microphotographs is that the LC sample appears to have a smaller grain size and it appear to contain fewer dark features in comparison. The grain boundaries are also slightly less clear in comparison.

The observed visual differences in the apparent grain size are quantified using grain size analysis for both specimens. To determine the grain size of each specimen, a total of 20 straight lines were drawn of which the first 10 were vertical lines of 0.3 mm in length and the latter half were horizontal lines of 0.5 mm. The results of the grain size analysis for both specimens are presented in Table 4.

Table 4. Grain size measurements

Line	Intersections, HC		Intersections, LC	
	0.3 [mm]	**0.5 [mm]**	**0.3 [mm]**	**0.5 [mm]**
1	17	34	24	37
2	22	38	22	33
3	18	32	24	35
4	17	30	19	36
5	20	31	23	34
6	18	32	24	29
7	19	34	20	31
8	17	30	19	31
9	23	28	22	32
10	22	29	20	26
***l* [mm]**	0,0155	0,0157	0,0154	0,0154
G	8,5	8,5	9	9
***STD* [mm]**	0,0018	0,00139	0,00153	0,00171
***CI-95 %* [mm]**	0,00129	0,00099	0,0011	0,00123
***E*rel [%]**	8,2	6,3	7,1	7,9

Based on the grain size measurements shown in Table 4, the average grain size is very small in both samples. The two specimens are relatively evenly matched in terms of grain size. However, since the mean lineal intercept length in the LC sample is right at the boundary between a grain size index 8.5 and 9, it was designated as a 9, which corresponds to mean grain diameters of 16.8 µm and 14.1 µm, respectively.

Although the difference in the measured grain size is relatively small, it is implied that the LC specimen will benefit more in terms of fatigue performance. The fine-grain size observed in both specimens is expected to be beneficial in terms of fatigue performance. According to Venturelli et al. (2018), a reduction in austenite grain size improves the mechanical properties including fatigue performance as well as the strain-hardening behaviour of Hadfield steel.

While the grain size analysis provided valuable insight into the structure of the specimen and its mechanical properties, grain size analysis, hardness testing and an optical microscope cannot reveal the presence of secondary phases and other features which may also influence the fatigue performance of Hadfield steel. Therefore, additional microstructural investigation was undertaken using SEM.

The SEM observations focused on identifying secondary phases and other microstructural features not clearly visible using an optical microscope. Figure 13 shows the microstructure of the HC specimen at different levels of magnification using the SE detector.

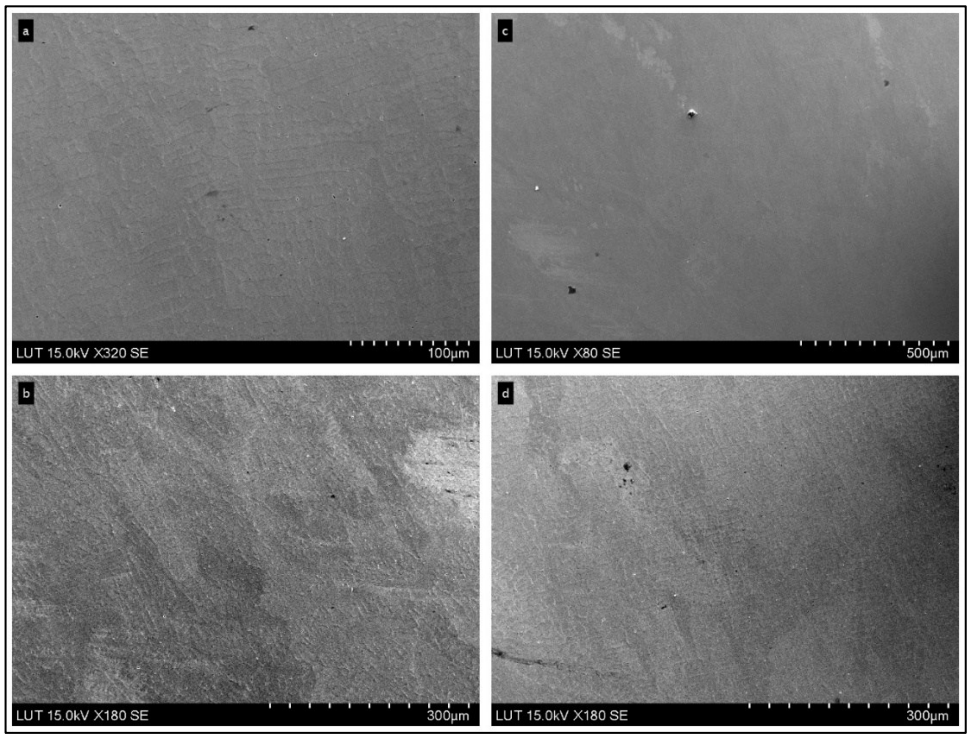

Figure 13. HC specimen SE a). Microstructure at x320 magnification, b). Microstructure at x180 magnification, c). Microstructure at x80 magnification, d). Microstructure 2 at x180 magnification.

In the HC sample shown by Figure (13a & 13c), the microstructure appears to consist in large part of an austenite matrix with sparsely distributed faint brighter regions that are approximately 100-300 µm lengthwise. All four photomicrographs also reveal similar darker features that were observed earlier in Figures 11 and 12.

A research paper by Gürol & Kurnaz (2020), showed that in Hadfield steel specimens with a higher carbon content, the fraction of carbide increases in the grains as well as grain boundaries even if Mn content is kept constant. Conversely, in the Hadfield steel specimens with a lower C content should contain less carbides. Figure 14 shows the microstructure of the LC specimen at different levels of magnification.

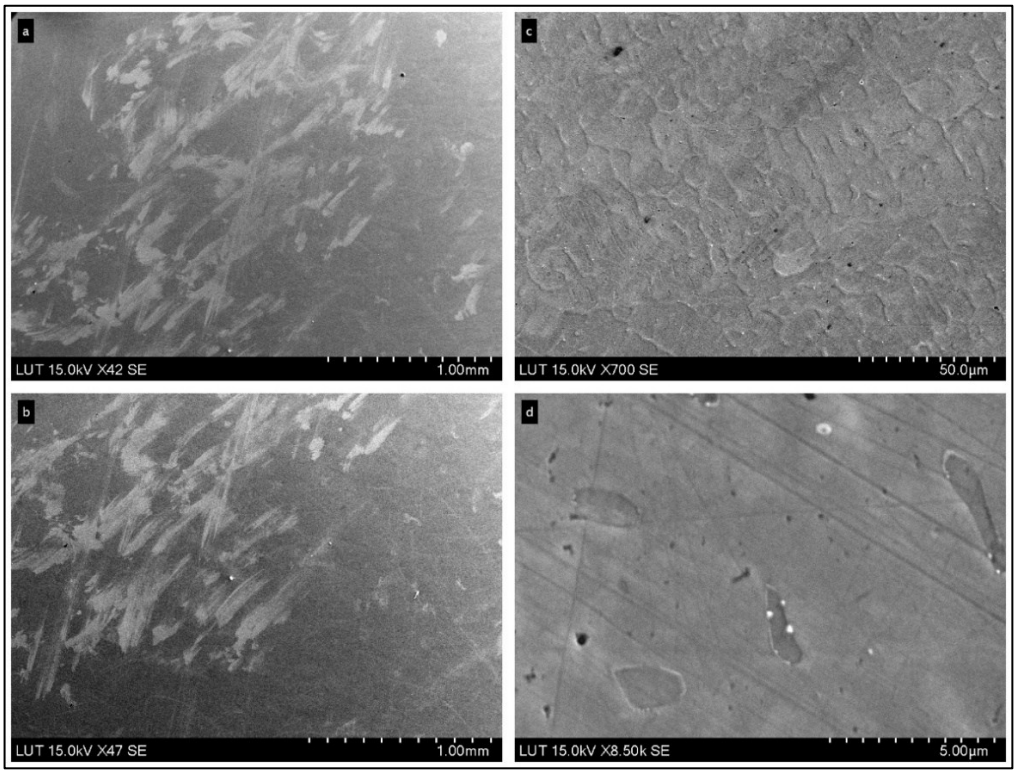

Figure 14. LC specimen SE a). Microstructure at x42 magnification, b). Microstructure at x47 magnification, c). Microstructure at x700 magnification, d). Microstructure at x8.5k magnification.

Whereas the HC specimen showed a small number of bright contrast patches, Figure (14a & 14b) shows the opposite. There are multiple areas both small and large. The brighter patches that are only visible using SE are most likely polishing artefacts due to their shape instead of secondary phases of the microstructure. The streaks appear to follow a curvilinear path similar to the motion employed during polishing.

In addition to the formation of carbides along grain boundaries, the microstructure of Hadfield steel can also contain small pearlite colonies adjacent to grain boundaries within the largely austenite matrix. These pearlite colonies form as a result of carbon rejection from austenite when the alloy is cooling. Towards the surface of a Hadfield steel specimen, a thin but hard martensitic layer can form as a result of the casting process while the material solidifies or even during heat treatment (Subramanyam et al. 1992, pp. 431-432).

To capture the presence of secondary phases and changes in the microstructure, general EDS mapping as well as point analyses were carried out. Figure 15 shows the microstructure including the grain boundaries of the HC specimen using the BSE detector.

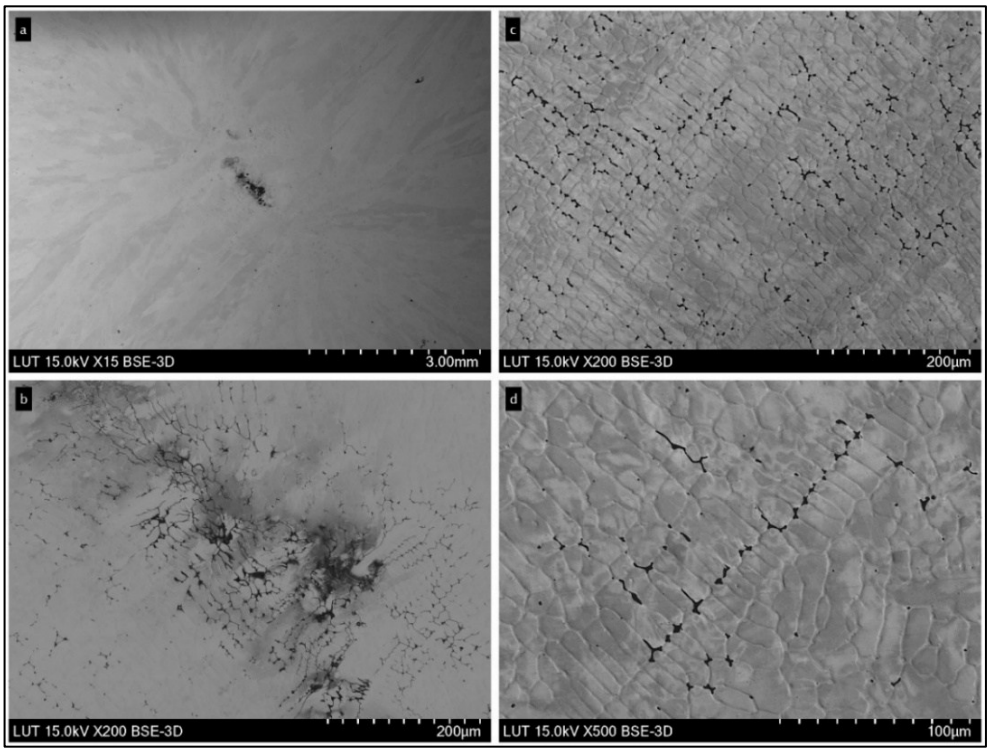

Figure 15. HC Specimen BSE a) General view of specimen, b) General view at x200, c). Grain boundaries at x200, d) Grain boundaries at x500

In the BSE images of the HC-specimen shown by Figure (15a), an overview of the cross-section reveals a concentration of darker features at the centre of the specimen. At higher magnifications, the darker features near the centre of the specimen reveal a network that aligns with the grain boundaries and interdendritic areas of the microstructure. As previous research has shown, Hadfield steel with a higher C content to be more prone to the formation of carbides along grain boundaries, the darker features observed in Figure 11 could correspond to these very carbides.

To investigate the chemical composition of these darker features, EDS was applied for the same region. In this thesis, EDS is used qualitatively to identify different elements and their composition; the reported values are semi-quantitative. It should be noted that the following

microstructural observations regarding chemical composition are highly localised, and should therefore be analysed with caution, as they can produce false-positive signals due to EDS low sensitivity to trace elemental concentrations, as well as low detectability of elements in comparison to Wavelength-Dispersive X-ray Spectroscopy (WDS) (Hamid 2018, p. 272). Figure 16 shows some regions where general EDS mapping as well as point analysis were performed on the HC specimen.

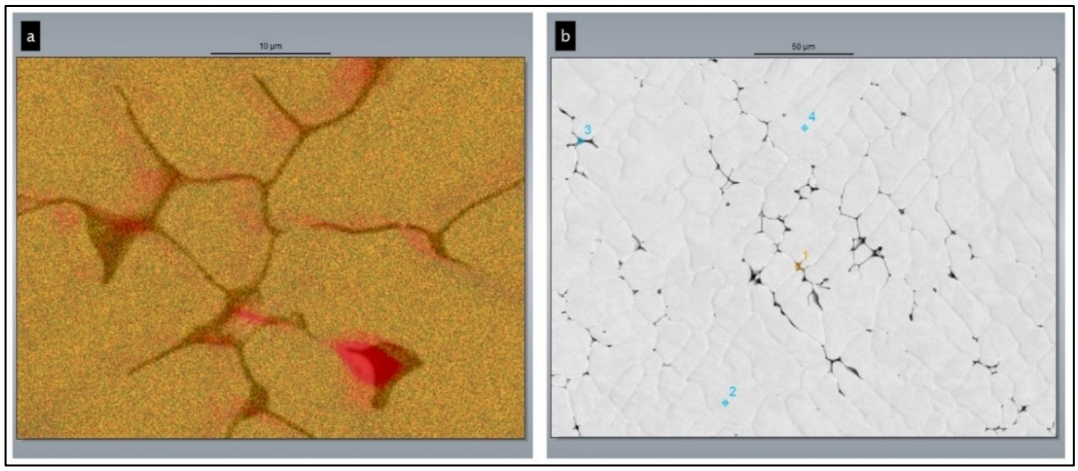

Figure 16. HC specimen a) General map, C (red) + Iron (Fe) (yellow), b) Point analysis of several areas

The general EDS map shown by Figure (16b) reveals that the quantity of C is not evenly distributed across the microstructure but rather segregated along the grain boundaries and adjacent areas whereas Fe appears to be evenly distributed throughout the matrix which is to be expected.

Point analysis of both the austenite matrix as well as a region in the vicinity of a grain boundary with segregated C is shown by Table 5.

Table 5. Point EDS analysis, HC specimen

Point	C [wt.-%]	Cr [wt.-%]	Mn [wt.-%]	Fe [wt.-%]
1	3.34	3.12	21.89	65.09
4	1.39	2.82	18.5	73.08

Based on the composition shown by Table 5, the segregated carbon located in the grain boundaries is approximately 2.5 times higher than in the austenite matrix which could indicate the presence of grain boundary carbides, likely alloyed cementite $(Fe, Mn)_3C$ in which Mn substitutes for Fe.

In contrast to the HC specimen, the LC specimen revealed noticeably less segregated carbon along the grain boundaries. The microstructure of the LC specimen with visible grain boundaries is presented in Figure 17.

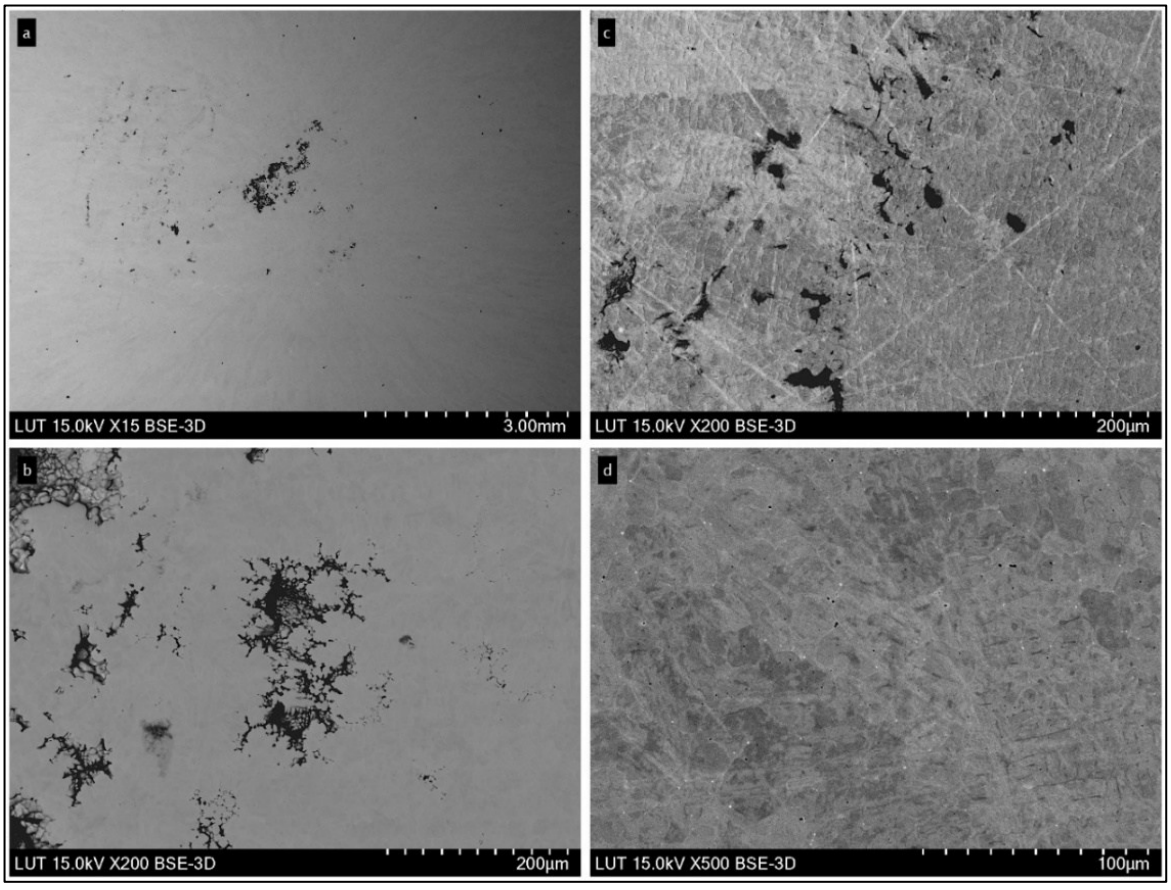

Figure 17. LC Specimen BSE a) General view of specimen, b) General view at x200, c). Grain boundaries at x200, d) Grain boundaries at x500

A preliminary comparison of Figure (15a) to Figure (17a) suggests that the LC sample contains a greater number of darker features in the centre of the specimen. However, upon a closer look using SEM, it becomes clear that the largest dark feature in Figure (17a) is in fact a void and not a constituent of the microstructure.

At higher magnification, the microstructure adjacent to the observed void appears largely uniform, with small scattered dark features similar to the ones found in the HC specimen. A comparison of Figures (15b & 15c) and Figures (17c & 17d) reveals that the grain boundaries of the LC specimen contain almost zero darker features. Rather, the darker features are clustered in pools of approximately 5-20 µm in diameter and as smaller dots within the matrix as well as grain boundaries and other interdendritic regions.

To investigate the chemical composition of the microstructural features in the LC specimen, EDS mapping and point analyses were carried out. Figure 18 shows some regions where general EDS mapping as well as point analyses were performed on the LC specimen.

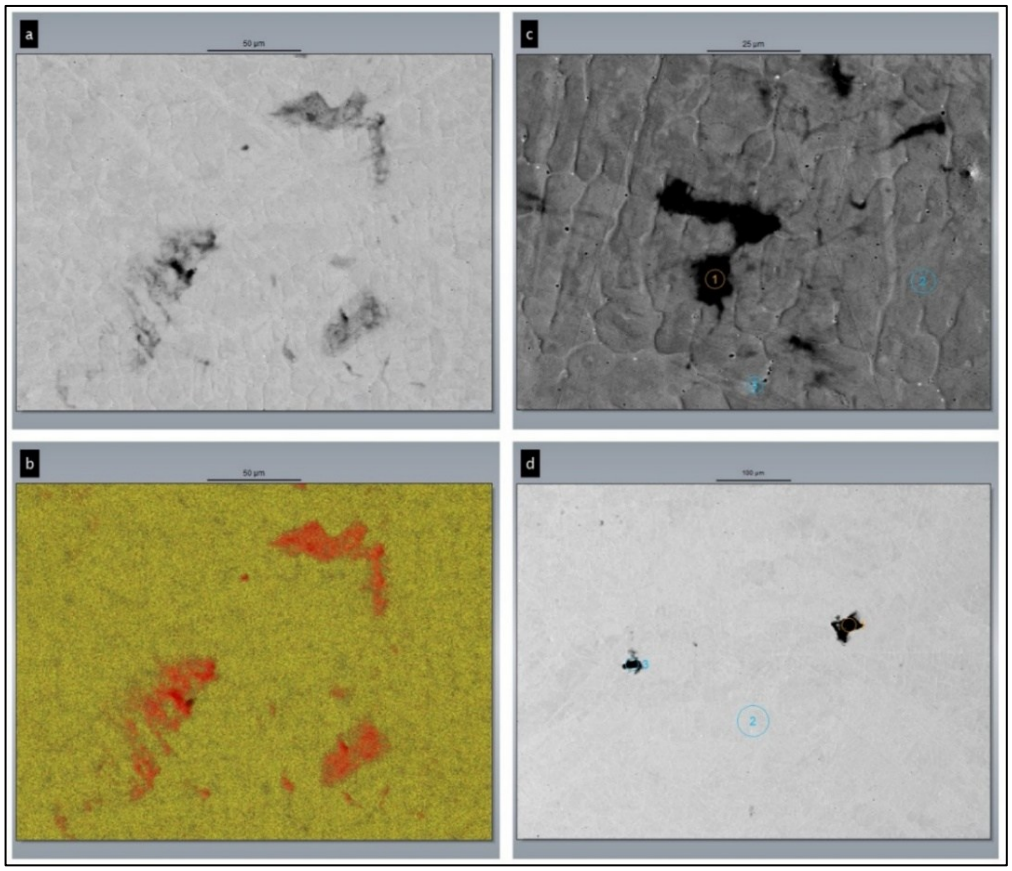

Figure 18. LC specimen a) General map b) General map, C (red) + Fe (yellow), c) Point analysis of several points, d) Point analysis of an arbitrary section.

In Figure 18b, the darker regions within the austenite matrix consist largely of carbon. However, Figure 18a reveals these regions to be very thin translucent films indicating that

they are not microstructural constituents such as precipitated carbide because secondary phases typically appear as solid features whereas in this instance the microstructure including individual grain boundaries of the LC specimen can be observed below the thin film of carbon.

Complementary to the EDS maps, point analyses were carried out comparing the composition of the austenite matrix as well as the different microstructural features. The results of the point analysis of the LC specimen are presented in Table 6.

Table 6. Point EDS analysis, LC specimen

Point	C [wt.-%]	Cr [wt.-%]	Mn [wt.-%]	Fe [wt.-%]
1, c	24.34	2.18	15.51	52.5
2, c	1.49	2.54	19.95	68.3
3, c	1.79	4.12	25.08	61.67
3, d	28.61	2.69	16.8	45.75

Based on the results of the point analyses in Table 6, points 2 and 3 in Figure 18c represent the austenite matrix, whereas points 1 in Figure 18c and point 3 in Figure 18d could either cautiously be designated as precipitated carbide or a similar carbon film as seen previously in Figure 18a.

Another observed difference between the two samples, besides their carbon content, is that more Al was detected in the LC variant by the EDS analysis. Although the Hadfield steel specimens in this study are not supposed to contain Al, EDS measured the Al content to be between 2-7 wt.-% in the LC specimen, and 0.4-3 wt.-% in the HC specimen, which may be the result of a local contamination, inclusion such as Al oxide, or simply a measurement error instead of an alloying element. The presence of Al in Hadfield steel could lead to the formation of κ-carbides, or $(Fe, Mn)_3AlC$ instead of alloyed cementite which is more common in Hadfield steels with a higher C content. According to Subramanyam et al. (1992, p. 432), increasing the Al content in Hadfield steel can also result in the formation of Al oxide (Al_2O_3), which is a hard ceramic. Additionally, Al content in excess of 5 % can make it difficult to stabilise the austenite phase, even with water quenching.

The presence of Al in Hadfield steel could potentially be negative in terms of its mechanical properties. Astafurova et al. (2007) observed that in single crystal specimens, the added Al increases SFE and results in the suppression of mechanical twinning, which is one of the two main deformation mechanisms of Hadfield steel. However, Al can also result in a higher yield strength as well as increase the rate at which work hardening occurs at small strains, but it comes at the expense of a lower tensile strength and work hardening rate at higher strain level. (Abbasi et al. 2009)

In closing, the metallographic investigation revealed clear differences between the HC and LC specimens. Because C and Mn are carbide-forming elements, the HC variant exhibited significantly more C and Mn segregation along the grain boundaries as evidenced by Figure 16a, which could cautiously be defined as alloyed cementite, or $(Fe, Mn)_3C$. Compared to the HC specimen, there was almost no segregated carbon in the LC specimen along the grain boundaries within the examined area. Instead, most of the C-rich signals using EDS point analysis coincided with small, isolated pools some of which appeared to be thin film-like layer on top of the mostly austenite matrix with occasional small features along the grain boundaries, which could coincide with carbide precipitate, likely alloyed cementite. If Al was present in the tested alloys, the carbide precipitate could also be κ-carbides, or $(Fe, Mn)_3AlC$. The observed microstructural features provide an important foundation for the interpretation of the fatigue results because different alloying elements as well as their quantity, influences the fatigue performance of Hadfield steel. However, it must be noted that the observed amount of Al in the specimens and its origin remains uncertain. As such, the influence of Al on the mechanical properties and fatigue performance should only be considered speculative, and all discussion related to the influence of Al on Hadfield steel is to be considered hypothetical in the scope of this thesis.

4.3 Fatigue

Building on the microstructural analysis in the previous subchapter, fatigue testing was performed on both HC and LC Hadfield steel specimens. The objective was to determine their fatigue performance and investigate how the microstructural differences between the two specimens caused by the difference in the quantity of C influences it.

The fatigue strength of the Hadfield steel specimens is determined by the fitting of the test data into a plot in the form of an S-N curve. The resulting S-N curves for both the HC and LC specimens is presented in Figure 19.

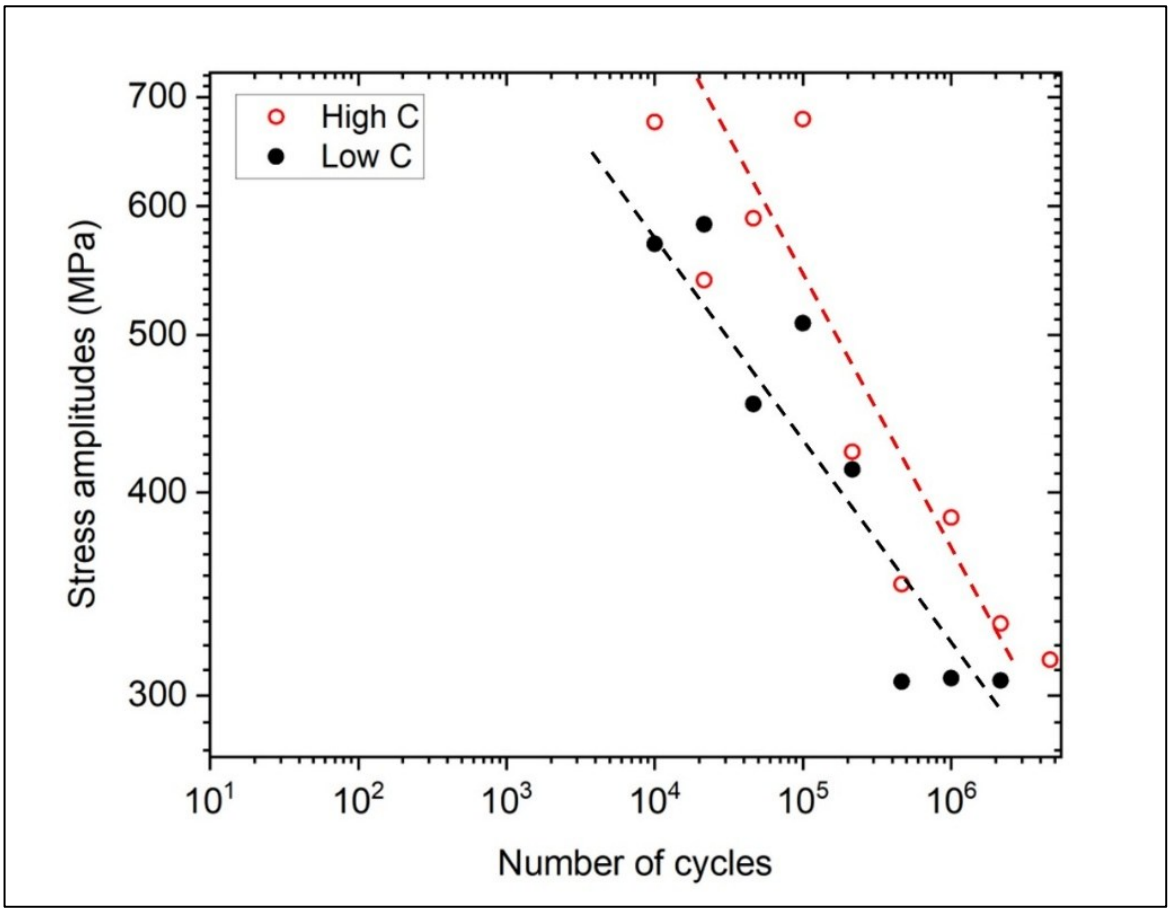

Figure 19. S-N Curve, HC and LC specimens

Based on the results obtained from the fatigue tests shown in Figure 19 indicates that the fatigue strength of the HC specimen is higher than that of the LC specimen. In the low-cycle regime at approximately 10^4 cycles, the fatigue strength of the HC specimen is approximately 680-690 MPa whereas the LC specimen is between 570-590 MPa based on the data corresponding to the stress amplitudes of each specimen. In the high-cycle regime, or at approximately $2x10^6$ cycles, the fatigue strengths are 330-335 MPa and 305-310 MPa respectively based on the datapoints at the 2 million cycle mark.

The low-cycle regime is fundamentally characterized by larger stresses and significant plastic deformation. In fact, up to 80 % of fatigue takes place during crack propagation whereas in the case of high-cycle fatigue the opposite holds true. In high-cycle fatigue, most of the time is spent on crack initiation and only up to 10 % for crack propagation with smaller test specimens. (Pook 2007, p. 31)

Given the clear difference in the fatigue performance between the two specimens, the underlying differences must be considered through the viewpoint of their physical properties. These include alloying elements, namely carbon content, microstructure and deformation mechanisms, all of which influence the fatigue strength of Hadfield steel.

The superior fatigue strength of the HC specimen can be explained by the improved tensile properties caused by the additional quantity of C. The influence of C content on the tensile properties of Hadfield steel has been studied by Subramanyam et al. (1990, pp. 1952-1954) and Chen et al. (2022). The yield- and tensile strength of austenitic manganese steel increases by approximately 50 MPa and 185 MPa respectively when the quantity of C is increased from 0.8 wt.-% to over 1 wt.-%. Beyond this range, added C does not offer any significant increases in the yield or tensile strength of the material. Increased yield- and tensile strength is consequently beneficial in terms of fatigue performance through increased DSA effect which enables dislocations to accrue resulting in a favourable strain hardening rate and improved tensile properties.

In the HC specimen, the slightly more intense DSA effect also results in a slightly harder material, as evidenced by the hardness test results, particularly towards the surface of the specimen. Increased C content improves the hardness of the material, and a harder surface is more resistant to crack initiation. This aligns with the research of Chen et al. (2017), who showed that the low-cycle fatigue performance of pre-hardened Hadfield steel improves because of increased dislocation density and the formation of deformation twins due to the hardening process.

On the other hand, increased amount of C can also produce negative effects as evidenced by Figures 15b and 15c showing large amount of segregated carbon along grain boundaries in the HC specimen. Increased C content promotes the formation of carbides along the grain boundaries, interdendritic regions, and the austenite matrix. The net effect of carbides is negative because they act as location from which fatigue cracks can initiate and propagate

to failure. Fatigue initiation and propagation along carbides is preferential because carbides by their nature lack ductility to accommodate the local plastic deformation during cyclic loading. Further, if the volume fraction of these carbides increases to a sufficient degree, the fracture mechanism can turn from ductile to brittle (Ueji et al. 2012). Another consideration is the increased SFE which delays the formation of deformation twins under cyclic loading which improves the fatigue performance by resulting in secondary boundaries along grain boundaries that act as locations where the growth of cracks slow down.

Besides C content, EDS analysis revealed that both specimens contain Al. However, as Al is not a part of their chemical composition, the detected amount is likely a measurement error, contamination or an inclusion. If Al was included in the Hadfield steel specimens, it could potentially play an important role insofar as Al can improve the yield strength of Hadfield steel, but it does so at the expense of tensile strength and work-hardening rate, as well as the fact that it increases SFE. For the LC specimen, the relatively lower quantity of C is beneficial in terms of fatigue performance due to the lower SFE. Moreover, if Al was included in the chemical makeup of the specimens, it could result in a situation where the formation of deformation twinning was suppressed thus negating its beneficial effects on fatigue performance.

On the other hand, according to Moshtaghi and Safyari (2021), the influence of SFE on the fatigue life of austenitic stainless steels is mostly uncorrelated. SFE is largely responsible for contributing to deformation mechanisms, specifically work-hardening.

However, the governing mechanism behind strain hardening in Hadfield steel is still debated in literature. According to Bańkowski et al. (2024), the work-hardening capacity is attributed in large part to deformation twinning. As deformation twins hinder the movement of dislocation, the implication is that they are beneficial in terms of improving fatigue performance but only to a certain degree. If work-hardening occurs in an uncontrolled manner, the net effect on fatigue life may be negative because it can result in unwanted cracks in the hardened surface layer of the base material that propagate until failure. Another contributing factor is DSA which according to Kang et al. (2014) is responsible for cyclic hardening through the C atoms in C-Mn clusters. The interaction of C atoms in C-Mn cluster reduces the mobility of dislocations during deformation. The relationship between deformation mechanisms and fatigue performance is complex but together, both deformation

twinning and DSA contribute to improved fatigue performance by delaying plastic deformation, but they may also accelerate it under special circumstances.

In summary, the better fatigue performance of the HC specimen compared to the LC specimen can be attributed mainly to its higher content of C which results in a higher yield- and tensile strength as well as surface hardness due to the DSA effect. The combination of these variables is an improved fatigue resistance at low- and high-cycle regime for the HC specimen. Although EDS detected Al in the specimens, it was not a part of their chemical composition, and therefore its influence on the mechanical properties cannot be determined conclusively. If Al was a part of the specimens, it could increase the yield strength of the LC specimen to offset the larger initial difference in the tensile properties, but it would also mitigate the formation of beneficial deformation twins at both high and low strains under cyclic loading. In the high-cycle regime, the fatigue strength of both specimens is closer to each other. This is likely a result of the increased number of grain boundary carbides in the HC specimen, which tend to act as paths for fatigue cracks to propagate. However, because the number of grain boundary carbides in the HC specimen is probably insufficient to result in a brittle microstructure, the HC specimen has a sufficiently ductile microstructure to outperform the LC specimen in terms of fatigue performance at both ends of the S-N curve. The disparity in fatigue strength at high-cycle regime remains small for both specimens. Consequently, machinery components that are subject to high- and very high cycle fatigue should be made from a lower C variant as the influence of C in the microstructure proves more deleterious at higher cycles. Conversely, for low-cycle fatigue, specimens with a higher content of C should be preferred due to their improved tensile properties.

5 Conclusions

The main objective of this thesis was to assess the fatigue performance of Hadfield steels with different C contents. Fatigue assessment was supported by microstructural analysis and hardness testing. The research objective was achieved by combining experimental fatigue testing with optical microscopy, as well as the use of SEM and EDS, and hardness measurements for the two test specimens.

Results of the fatigue assessment revealed a clear difference in the fatigue performance between the HC and LC specimens. The fatigue strength of the HC specimen was higher in both low-cycle and high-cycle regimes. At approximately 10^4 cycles, the fatigue strength of the LC specimen was almost 100 MPa less than the HC specimen. Towards the $2x10^6$ cycle mark, the disparity in the respective fatigue strength narrowed to approximately 25 MPa. The improved fatigue strength of the HC specimen was attributed to the increased quantity of C, which improves the tensile properties of Hadfield steel through the DSA effect.

The microstructural observations were used to gather insight about the differences between the two specimens. Grain size analysis revealed a small difference in the average grain size, which would have only a minor effect on fatigue performance in favour of the LC specimen. Microhardness measurements proved that the influence of carbon is positive in terms of improved hardness. However, SEM and EDS showed significant amounts of segregated C along the grain boundaries of the HC specimen, whereas the LC specimen showed significantly less C segregation. Based on the EDS analysis, the LC specimen also revealed a significantly increased amount of Al, which is likely a measurement error, contamination, or an inclusion because Al is not a part of the chemical composition of either specimen. If Al was a chemical constituent of the tested specimens, it could increase the yield strength of the alloy but at the expense of tensile strength. Increased Al also increases the SFE, which suppresses the formation of deformation twins, which act as barriers that slow down the propagation of crack growth. If Al was a constituent of the microstructure, deformation twinning could be even less likely to occur in the LC specimen, lowering its fatigue strength further. However, since there was not supposed to be Al as a part of the chemical composition of the tested alloys, its influence on the fatigue life of either specimen cannot be determined.

As a concluding remark, based on the results of this thesis Hadfield steel is more than suitable for use in machinery components that are subject to cyclic loads. For machinery components that are expected to operate under high stresses and in the low-cycle regime, an alloy with a higher quantity of C is preferred. Conversely, a machinery component subject to stresses below the yield strength of the material and cycles in excess of $2x10^6$, an LC variant is preferred.

While the conclusions appear promising, there exists limitations in this thesis. One notable limitation is the use of EDS alone for quantitative analysis of microstructures chemical element distribution and for identifying secondary phases. The wt.-% values presented in this work represent a reasonable trend of the actual chemical composition instead of conclusive proof, but the EDS results could be verified using a secondary method such as WDS combined with electron probe microanalysis (EPMA) to bolster the veracity of the results. Similarly, X-ray diffraction (XRD) could be used to complement the EDS mapping and point analysis to observe secondary phases in the microstructure.

Another limitation of this thesis includes the fact that only a few specimens were tested between the 2 different variants. Additional microstructural analysis could also be included post-fatigue testing to investigate the degree to which deformation twinning played a role in both specimens. In the future, the role of Al in suppressing deformation twinning could be investigated to determine the optimal ratio for improved yield strength while minimising SFE in Hadfield steels that contain Al, given that the presence of Al is first verified. Furthermore, the influence of SFE on the fatigue performance of Hadfield steel could be studied. While contrary evidence was shown between the fatigue resistance of austenitic stainless steels and SFE, no such conclusion can be drawn based on the information gathered within this work, because Hadfield steel differs from austenitic stainless steels. Other future work could also encompass a study of a machinery component, such as the tooth of a crusher made from Hadfield steel which undergoes very high-cycle fatigue in combination with repeated impacts during operation. The complex geometry and variable service loads would result in a multi-axial stress state bridging the gap between the fatigue performance obtained under laboratory conditions and in practice.

References

Abbasi, M., Kheirandish, S., Kharrazi, Y. & Hejazi, J. 2009. The fracture and plastic deformation of aluminum alloyed Hadfield steels. Materials Science and Engineering A 513-514 72-76. Available: https://doi-org.ezproxy.cc.lut.fi/10.1016/j.msea.2009.02.023

Andersson, H. 2021. Metal Fatigue Principles and Analyses: A Compendium. Available: https://urn.kb.se/resolve?urn=urn:nbn:se:ri:diva-56967

Anderson, T. L. 2005. Fracture Mechanics: Fundamentals and Applications. 3rd ed. Boca Raton (FL): Taylor & Francis.

Anijdan, M. S. H. & Sabzi, M. 2018. The Effect of Heat Treatment Process Parameters on Mechanical Properties, Precipitation, Fatigue Life and Fracture Mode of an Austenitic Mn Hadfield Steel. Journal of materials engineering and performance. 27 (10), 5246-5253. Available: https://doi.org/10.1007/s11665-018-3625-y

Arghavan, A., Kazem, R. K. & Asfarjani, A. A. 2011. Investigating Effect of Industrial Coatings on Fatigue Damage. Applied Mechanics and Materials 87. pp 230-237. Available: https://doi.org/10.4028/www.scientific.net/AMM.87.230

Astafurova, E. G., Tukeev, M. S. & Chumlyakov, Y. L. 2007. The effect of aluminum alloying on strength properties and deformation mechanisms of the (123) Hadfield steel single crystals. Russian physics journal. 50(10), p. 959-963. Available: https://doi.org/10.1007/s11182-007-0139-8

Bańkowski, D., Mlynarczyk, P. S., Depczyński, W. & Bolanowski, K. C. 2024. The Effect of Work Hardening on the Structure and Hardness of Hadfield Steel. Archives of foundry engineering 24.1:14. Available: https://doi.org/10.24425/afe.2024.149246

Bathias, C. & Pineau, A. 2010. Fatigue of materials and structures. London: ISTE. Available: https://app.knovel.com/hotlink/pdf/id:kt009XOP2C/fatigue-materials-structures/introduction-fatigue

Canadinc, D., Efstathiou, C. & Sehitoglu, H. 2008. On the negative strain rate sensitivity of Hadfield steel. Scripta Materialia 59, no. 10: 1103-1106. Available: https://doi.org/10.1016/j.scriptamat.2008.07.027

Chen, C., Lv, B., Wang, F. & Zhang, F. 2017. Low-cycle fatigue behaviors of pre-hardening Hadfield steel. Materials science & engineering. A, Structural materials: properties, microstructure and processing. 695 144-153. Available: https://doi.org/10.1016/j.msea.2017.03.107

Chen, C., Ma, H., Wang, F., Yang, Z., Zhang, F & Yan, Z. 2022. Influence of Carbon Content on Tensile Properties of Pure High Manganese Austenitic Steel. Coatings, 12, 1622. Available: https://doi.org/10.3390/coatings12111622

Dhar, S., Danielsen, H. K,. Fæster, S., Rasmussen, C., Zhang, Y. & Juul Jensen, D. 2019. Crack formation within a Hadfield manganese steel crossing nose. Wear, 438, Article 203049. Available: https://doi.org/10.1016/j.wear.2019.203049.

Dowling, N. E. 1979. Notched Member Fatigue Life Predictions Combining Crack Initiation and Propagation. Fatigue & Fracture of Engineering Materials & Structures, 2: 129-138. Available: https://doi.org/10.1111/j.1460-2695.1979.tb01349.x

Dowling, N. E., Katakam, S. P. & Narayanasamy, R. 2013. Mechanical Behavior of Materials: Engineering Methods for Deformation, Fracture, and Fatigue. 4th ed., international ed. Harlow: Pearson Education.

Ellyin, F. 1997. Fatigue Damage, Crack Growth and Life Prediction. London. Chapman & Hall. Available: https://doi.org/10.1007/978-94-009-1509-1

Fatemi, A, & Yang, L. 1998. Cumulative Fatigue Damage and Life Prediction Theories: A Survey of the State of the Art for Homogenous Materials. International journal of fatigue. 20, no. 1: 9-34. Available: https://doi.org/10.1016/S0142-1123(97)00081-9.

Feng, X. Y., Zhang, F. C., Zheng, C. L. & Lü, B. 2013. Micromechanics behavior of fatigue cracks in Hadfield steel railway crossing. Sci. China Technol. Sci. 56, 1151-1154. Available: https://doi.org/10.1007/s11431-013-5181-x

Frost, N. E., Pook, L. P. & Marsh, K. J. 1999. Metal Fatigue. Dover Publications. Available: https://app.knovel.com/hotlink/toc/id:kpMF000004/metal-fatigue/metal-fatigue

Gdoutos, E. E. 2020. Fracture Mechanics: An Introduction. 3rd ed. Cham: Springer International Publishing. Available: https://doi.org/10.1007/978-3-030-35098-7

Gurney, T. 2006. Cumulative damage of welded joints. Woodhead Publishing. Available: https://app.knovel.com/hotlink/pdf/id:kt008WPHZ1/cumulative-damage-welded/front-matter

Gürol, U. & Kurnaz, S. C. 2020. Effect of Carbon and Manganese Content on the Microstructure and Mechanical Properties of High Manganese Austenitic Steel. Journal of Mining and Metallurgy. 56(2), 171-182. Available: https://doi.org/10.2298/JMMB191111009G

Harzallah, R., Mouftiez, A., Felder, E., Hariri, S. & Maujean, J. -P. 2010. Rolling contact fatigue of Hadfield steel X120Mn12. Wear. 269 (9), 647-654. Available: https://doi-org.ezproxy.cc.lut.fi/10.1016/j.wear.2010.07.001

Kang, J., Zhang, F. C., Long, X. Y. & Lv, B. 2014. Cyclic deformation and fatigue behaviors of Hadfield manganese steel. Materials Science & Engineering A 591, 59-68. Available: https://doi.org/10.1016/j.msea.2013.10.072.

Karaman, I., Sehitoglu, H., Gall, K., Chumlyakov, Y. I. & Maier, H. J. 2000. Deformation of single crystal Hadfield steel by twinning and slip. Acta Materialia. 48 (6), 1345-1359. Available: https://doi.org/10.1016/S1359-6454(99)00383-3.

Kirk, D. 2023. Shot Peeners' Magic Steel Mangalloy, The Shot Peeners magazine, Vol 37, Issue 4. Academic Study. Coventry University. Referred 17.01.2025. Available: https://www.shotpeener.com/library/detail.php?anc=2023036

Lee, Y-L., Pan, J., Hathaway, R. & B, Barkey, M. E. 2005. Fatigue Testing and Analysis - Theory and Practice. Chantilly: Elsevier. Available: https://ebookcentral.proquest.com/lib/lut/detail.action?docID=226735

Maiti, S. K. 2015. Fracture Mechanics: Fundamentals and Applications. Cambridge: Cambridge University Press. Available: https://research-ebsco-com.ezproxy.cc.lut.fi/linkprocessor/plink?id=283f600e-47fa-39ef-9b2d-27569489841c

Miekk-oja, H. M., Lindroos, V. Sulonen, M. Veistinen, M. 1986. Uudistettu Miekk-ojan Metallioppi. Otava

Milella, P. P. 2024. Fatigue and Corrosion in Metals. 2nd ed. Cham: Springer International Publishing. Available: https://doi.org/10.1007/978-3-031-51350-3

Moshtaghi, M. and Safyari, M. 2021. Effect of Work-Hardening Mechanisms in Asymmetrically Cyclic-Loaded Austenitic Stainless Steels on Low-Cycle and High-Cycle Fatigue Behavior. Steel research international. 92 (1). Available: https://doi-org.ezproxy.cc.lut.fi/10.1002/srin.202000242

Moshtaghi, M. & Sato, S. 2019. Characterization of Dislocation Evolution in Cyclically Loaded Austenitic and Ferritic Stainless Steels via XRD Line-Profile Analysis. ISIJ International, 59(9) 1591-1598. Available: https://doi.org/10.2355/isijinternational.ISIJINT-2019-077

Nicholas, T. 2006. High Cycle Fatigue – A Mechanics of Materials Perspective. Oxford: Elsevier. Available: https://app.knovel.com/hotlink/pdf/id:kt00BFIZDA/high-cycle-fatigue-mechanics/front-matter

Paris, P. C. 1962. The Growth of Cracks Due To Variations In Load. Lehigh Library Digital Collections. Available: https://preserve.lehigh.edu/lehigh-scholarship/graduate-publications-theses-dissertations/theses-dissertations/growth-cracks.

Pook, L. P. 2007. Metal Fatigue: What it is, Why it Matters. Dordrecht: Springer. Available: https://doi.org/10.1007/978-1-4020-5597-3

Safyari, M. and Moshtaghi, M. 2025. Multiscale fatigue assessment of wire arc additively manufactured aluminium alloys with experimental and simulation approach. Welding in the world. 69 (8), 2269-2278. Available: https://doi.org/10.1007/s40194-025-01996-6

Schijve, J. 2009. Fatigue of Structures and Materials. Dordrecht: Springer Netherlands. Available: https://doi.org/10.1007/978-1-4020-6808-9

Schilke, M., Ahlström, J. & Karlsson, B. 2010. Low cycle fatigue and deformation behavior of austenitic manganese steel in rolled and as-cast condition. Procedia Engineering 2, 623-628. Available: https://doi.org/10.1016/j.proeng.2010.03.067.

Schütz, W. 1996. A History of Fatigue. Engineering Fracture Mechanics 54 (2), pp. 263-300. Available: https://doi.org/10.1016/0013-7944(95)00178-6.

SFS-EN 643:2024. 2024. Steels. Micrographic determination of the apparent grain size. Helsinki: Finnish Standards Association SFS. 52 pages.

Stephens, R. I., Fatemi, A., Stephens, R. R. & Fuchs, H, O. 2001. Metal Fatigue in Engineering (2nd Edition). John Wiley & Sons. Available: https://app.knovel.com/hotlink/toc/id:kpMFEE0008/metal-fatigue-in-engineering/metal-fatigue-in-engineering

Subramanyam, D. K., Grube, G. W. & Chapin, H. J. 1992. Metals Handbook. Vol 9, Metallography And Microstructures. 9. Ed. Materials Park (OH): ASM International. pp. 428-438.

Subramanyam, D. K., Swansiger, A. E. & Avery, H. S. 1990. Metals Handbook. Vol 1, Properties and Selection: Irons, Steels and High-Performance Alloys. 10. ed. Materials Park (OH): ASM International. pp. 1951-2004.

Sun, C-T. 2011. Fracture Mechanics. 1st ed. Chantilly: Elsevier Science & Technology. Available: https://doi.org/10.1016/C2009-0-63512-1.

Tecza, G & Garbacz-Klempka, A. 2016. Microstructure of Cast High-Manganese Steel Containing Titanium. Foundry Engineering. ISSN (1897-3310), (16) 163-168. Available: https://www.researchgate.net/publication/309188045_Microstructure_of_Cast_High-Manganese_Steel_Containing_Titanium

Ueji, R., Kondo, D., Takagi, Y., Mizuguchi, T., Tanaka, Y. & Shinagawa, K. 2012. Grain size Effect on high-speed deformation of Hadfield steel. Journal of Material Science, 47:7946-7953. Available: https://doi.org/10.1007/s10853-012-6604-y

Ul-Hamid, A. 2018. A Beginners' Guide to Scanning Electron Microscopy. Cham: Springer International Publishing. Available: https://doi.org/10.1007/978-3-319-98482-7

US 8,753,565 B2. 2014. Hadfield Steel. Oguiza, C. 13/325,223. 14.12.2011. Published 14.06.2012.

Venturelli, B. N., Albertin, E. & Azevedo, C. R. F. 2018. The effect of the austenite grain refinement on the tensile and impact properties of cast Hadfield steel. Material Research 21(5). Available: https://doi.org/10.1590/1980-5373-MR-2018-0069

Wulpi, J. & Miller, B. 2013. Understanding how Components Fail, 3rd Edition. ASM International. Available:

https://app.knovel.com/hotlink/toc/id:kpUCFE0001/understanding-how-components/understanding-how-components

Xiong, R., Peng, H., Wang, S., Si, H. & Wen, Y. 2015. Effect of stacking fault energy on work hardening behaviors in Fe-Mn-Si-C high manganese steels by varying silicon and carbon contents. Materials and Design, Volume 85, 707-714. Available: https://doi.org/10.1016/j.matdes.2015.07.072.

Zehnder, A. T. 2012. Fracture Mechanics. Dordrecht: Springer Netherlands. Available: https://doi.org/10.1007/978-94-007-2595-9